Schweizerische Eidgenossenschaft
Confédération suisse
Confederazione Svizzera
Confederaziun svizra

Department of the Environment,
Transport, Energy and Communication DETEC

Swiss Federal Office of Energy SFOE
Energy Research

Final report

Clean-PV

Electrodynamic Cleaning System for PV Industry

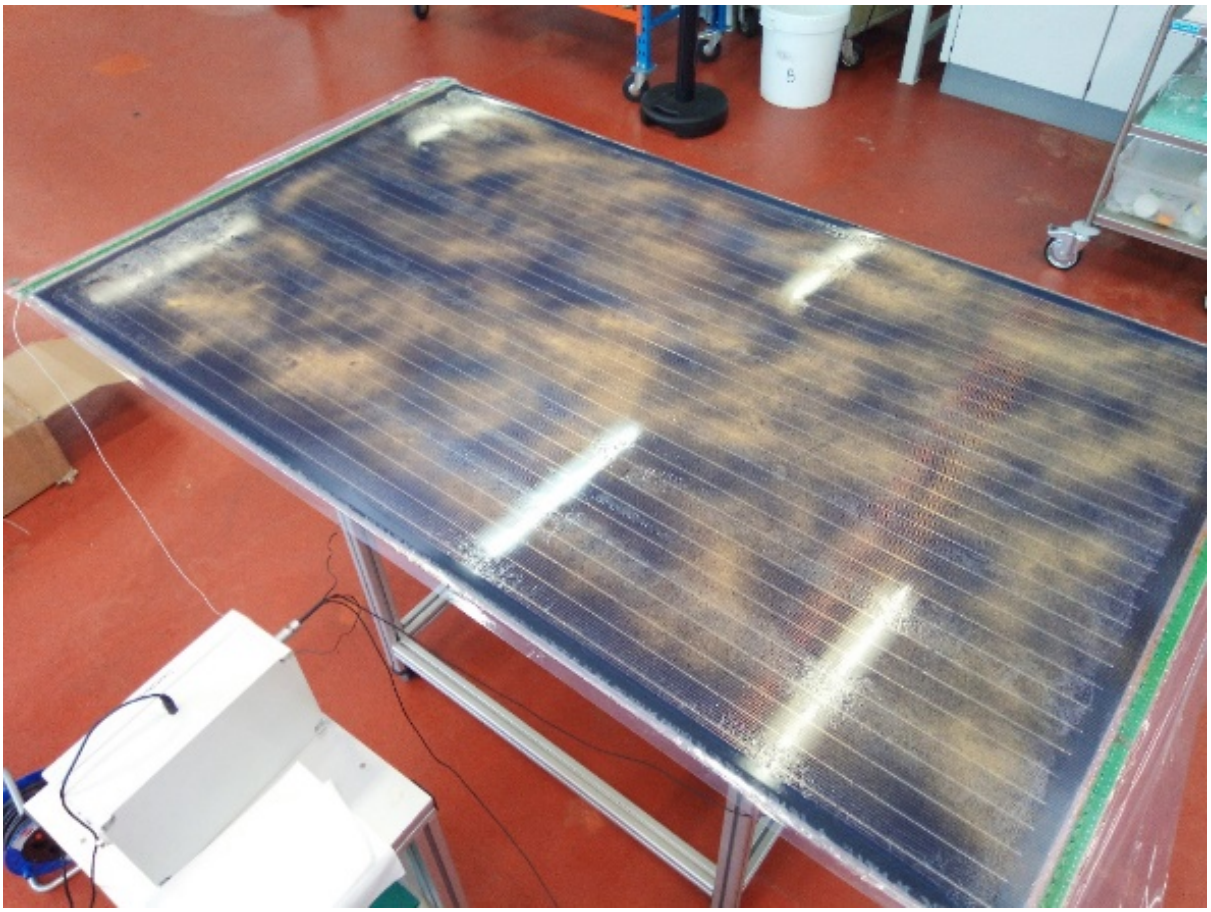

Date: 17 January 2020

Place: Neuchatel

Publisher:
Swiss Federal Office of Energy SFOE
Research Programme
CH-3003 Bern
www.bfe.admin.ch
energieforschung@bfe.admin.ch

Co-financed by:
CSEM SA
Rue Jaquet-Droz 1
CH-2002 Neuchatel
www.csem.ch

Agent:
CleanFizz SA
Rue Pré-de-La-Fontaine 15
CH-1217 Meyrin
www.CleanFizz.com

Authors:
Antonin Faes, CSEM SA, afs@csem.ch
Matthieu Despeisse, CSEM SA, mde@csem.ch
George McKarris, CleanFizz SA, George.mckarris@cleanfizz.com

SFOE head of domain: Name Projektbegleiter/in BFE gemäss Vertrag, email@adresse.ch
SFOE programme manager: Name Projektbegleiter/in BFE gemäss Vertrag, email@adresse.ch
SFOE contract number: SI/501790-01

Summary

The Clean-PV project pushes the anti-soiling electro-dynamic cleaning system (EDS) technology from CleanFizz to industrial size. Before the project small electrode of 20 by 20 cm^2 were the standard, now the standard PV module with 60 cells can be covered with CleanFizz technology. Modelling of electro-dynamic electrode and particle trajectory enable to optimize the EDS electrode and high voltage electronics. Combining field test, cost of washing PV and cost of EDS system production, demonstrated the bankability of CleanFizz technology.

Zusammenfassung

Das Projekt Clean-PV hat die Technologie von CleanFizz ermöglicht, mit seiner auf Hochspannung basierenden Technologie für die elektro-dynamische Sandreinigung einen industriellen Maßstab zu erreichen. Vor dem Projekt waren nur Proben mit einer Größe von 20 x 20 cm^2 möglich, jetzt können die CleanFizz-Elektroden handelsübliche PV-Module abdecken. Die Elektrodensimulation für die elektrodynamische Reinigung sowie die Partikelbahn haben das Elektrodensystem und die Hochspannungsquelle optimiert. Durch die Kombination von Feldtests, den Reinigungskosten der Solarmodule und den Kosten für die Herstellung des elektro-dynamischen Reinigungssystems konnte die wirtschaftliche Rentabilität der CleanFizz-Technologie nachgewiesen werden.

Résumé

Le projet Clean-PV a permis à la technologie de CleanFizz, basée sur de la haute tension pour un nettoyage électro-dynamique du sable, d'atteindre une dimension industrielle. Avant le projet, uniquement des échantillons de taille limitée à 20 par 20 cm^2 étaient possibles, maintenant les électrodes de CleanFizz peuvent couvrir des modules PV de tailles commerciales. La simulation des électrodes pour le nettoyage électro-dynamique ainsi que la trajectoire des particules ont permis d'optimiser le système d'électrode et la source de haute tension. En combinant des tests sur le terrain, le cout de nettoyage des panneaux solaires et le cout de production du système de nettoyage électro-dynamique, il a été possible de démontrer la rentabilité économique de la technologie de CleanFizz.

Seite absichtlich frei

Contents

List of abbreviations

CSP	Concentrated Solar Power
EDS	Electro-Dynamic cleaning System
ETFE	Ethylene tetrafluoroethylene
FF	Fill-Factor
GUI	Graphical User Interface
Isc	Short circuit current density
ITO	Indium Tin Oxide
OPR	Output Power Restoration
PCB	Printed Circuit Board
PV	Photovoltaics
s-DRE	Static dust removal efficiency
Voc	Open circuit voltage
WE	Wire Electrode

1 Introduction

1.1 Background / State of the art

A large market for photovoltaics (PV) and concentrated solar power (CSP) using mirrors is to be located in desert regions: while these regions represent more than 30% of the total earth land surface, the annual solar energy in such regions is typically two times higher than the average annual radiation in central Europe. The major limitation for PV electricity production in desert is the soiling due to sandstorm and dust accumulation at the PV module surface, which can reduce the power output of a power plant by up to 28% in only 7 days [1], thus requiring frequent cleaning of the surface of the PV modules or CSP mirrors.

Today solutions for cleaning represent important additional costs and need to be adapted in type and in frequency for each solar project. In addition, these solutions can consume diesel, rare purified water, costly equipment and manpower. The different current approaches are (1) fully manual, (2) mechanically assisted manual cleaning, (3) fully mechanical (with robots) with or without water or (4) modules with anti-soiling coatings [2]. Their main issue is the availability in desert location of clean and non-salted water as cleaning can consume between 7 to 20 m^3 of water per MWp per wash [3] and because mechanical cleaning without water can scratch and damage the solar panel or mirror surface. Anti-soiling coatings are working well for locations where rain occurs but they can have limited lifetime of few months due to coating erosion during cleaning or sandstorms [4].

An alternative cleaning approach is developed by using variable high voltage (in the order of kV) applied to dedicated electrodes integrated in the device, which charge the dust particles at the surface of the operated device. Dust particles can then be repulsed thanks to the Coulomb force and move out of the device surface following traveling waves. EDS is composed of multiple electrodes with variable voltages that can create standing or travelling electrostatic waves. For creating traveling waves, EDS with three or more electrodes are needed. Indoor tests show that up to 98 % of the sand can be removed in tens of seconds without using neither water nor mechanical cleaning [4 – 6]. First demonstration of particles transport using variable electric field was shown by Masuda et al. [7]. This approach was used for many different applications like dust removal for lunar and Martian exploration missions [8, 9] or for fusion reactors [10], particles supply in Xerography [11, 12] and bubbles or blood cells motion in dielectric liquids [13, 14]. The naming of this approach is as numerous as the number of its applications: electric curtain, electrodynamic screen, electrodynamic dust shield or electrostatic cleaning systems. In this report, electrodynamic cleaning system (EDS) will be used.

When alternated high voltage pulses are applied to only two independent electrodes, a standing wave is formed over the surface and the particles are moved forth and back due to the variable electric field: in this case gravity and wind are needed for efficient cleaning over large surfaces [5]. In case of three or more electrodes, a traveling wave can be generated and can move the particles even on horizontal surface (see Fig. 1) [4]. Modeling of electrodynamic cleaning system for better understanding and optimization of the design and process was already done by different institutes [9, 10, 11, 16, 17].

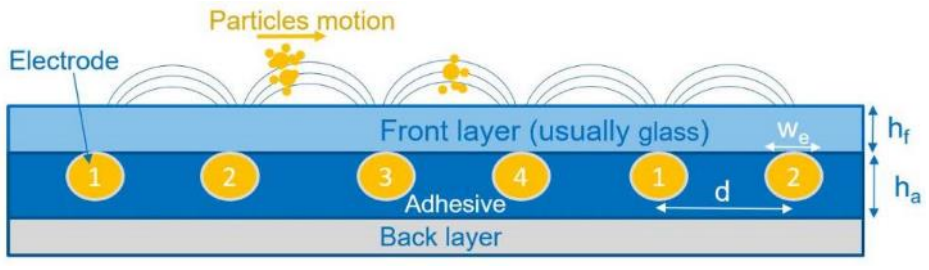

Fig. 1. Cross-section scheme of an electrodynamic system (EDS) for dust cleaning using 4 wire electrodes (WE) to create the traveling-wave.

1.2 Motivation of the project

Today only small scale demonstrators has been presented without real upscaling and production possibility. In literature, the electrode design can vary from standard interdigitated electrical line (in particular for standing wave) [4] to spiral design [15]. The voltage difference between electrodes usually varies between 0.9 and 7 kV. This induces an electrostatic field between electrodes of 0.14 to 3 kV/mm (kV/mm). The frequency is practically varied from 1 to about 100 Hz; at higher frequency the particles cannot follow the field variation. Various fabrication processes can be used for the conductive electrodes such as using copper wire, silver screen-printed or inkjet-printed lines, silver or indium-tin oxide (ITO) layers deposited by physical vapour deposition (PVD) and patterned [4 - 6]. The electrode pitch may range between 0.5 to 7 mm. The front dielectric layer is usually made of a thin polymer film [18] or a thin glass of 0.1 mm. One of the thicker front layers is reported by Guo and Javed with a 0.315 mm thick glass plus a 0.055 mm thick tape [6]. Usually samples with an area of 10 x 10 to 15 x 15 cm^2 are presented. Larger samples of 32 x 56 cm^2 in surface are presented by Kawamoto and Shibata [5] while Guo and Javed presented upscaling of the electrode to 60 x 120 cm^2 but not fully covered by a front glass [6].

1.3 Goals

The main goal of this project is to demonstrate an upscaling of the EDS at a standard PV module size, i.e. 60 c-Si solar cells of 1 meter by 1.6 meter, with a cost effective industrial process possible for EDS technology. Optimization of the electrode design and of electrodynamic process are fundamental goals of this project. Modeling of the electric field and particles displacement during EDS are of great interest for the further optimization. Combination of EDS, using low current and high voltage, with electrode heating, using high current and low voltage is important for reaching high cleaning efficiency. If the PV module reach the dew point, condensation will form at the PV glass surface. When the dust are wetted, cementation occurs that agglomerate the particles and which make EDS inefficient. Reliability of the demonstrator electrode will be also a goal to show equivalent long life-time as PV solar panels.

2 Approach and methodology

2.1 Sample fabrication

Various sample configurations for EDS electrode manufacturing were tested.

1. Spiral designs (see Fig. 3.2a) were done directly on the glass used as front electrode meaning that these electrode arrangements could be laminated on the front side of a PV module. Spiral design were done following two different processes:
    a. The first approach is based on sputtering technique of ITO (of 100 Ω/sq) followed by hotmelt inkjet and etch-back of ITO.
    b. The second approach to target upscaling of the etching process used after ITO sputtering to avoid large etching bath for the PV glasses. The patterning uses screen-

printing process of resist for sand-blasting application. After sand blasting the resist is peeled of and the glass is ready to be laminated (see Fig. 3.3 and 3.4).

2. Wire-electrode (WE) design (see Fig. 3.2b) were the different electrodes are parallel and go through the full sample surface.
    a. WE can be buid using fixed wire that are soldered on printed circuit board (PCB) on each side of the module (see Figure 3.5). The sample fabrication use paralel wire arrangement with a pitch of 2 to 8 mm, that are fixed by soladering on PCB. These wire are then laminated with thin glass of ETFE front-sheet.
    b. These wire-electrodes can be made of hybrid meshes proposed by SEFAR and composed of organic fibers and as conductive metallic wires (see Fig. 3.6).
    c. Wire electrode similar to point 2a and with connection on both sides that could be used both for EDS and heating purpose.

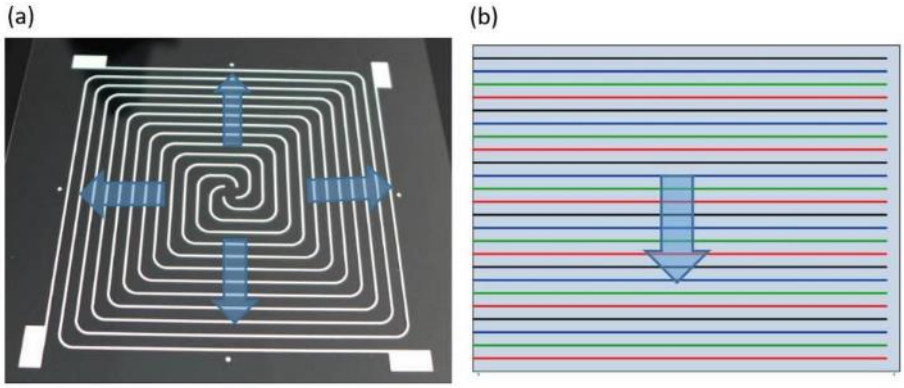

Fig. 3.2. (a) Picture of spiral electrode design (b) scheme of wire electrode (WE) design. Arrows represent the particles motion directions for horizontal samples, in all directions starting from center for

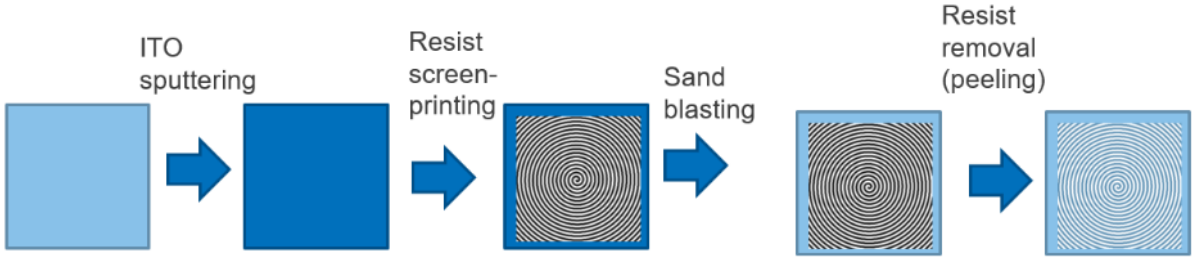

Fig. 3.3. Scheme of the process of spiral design fabrication using sand-blasting.

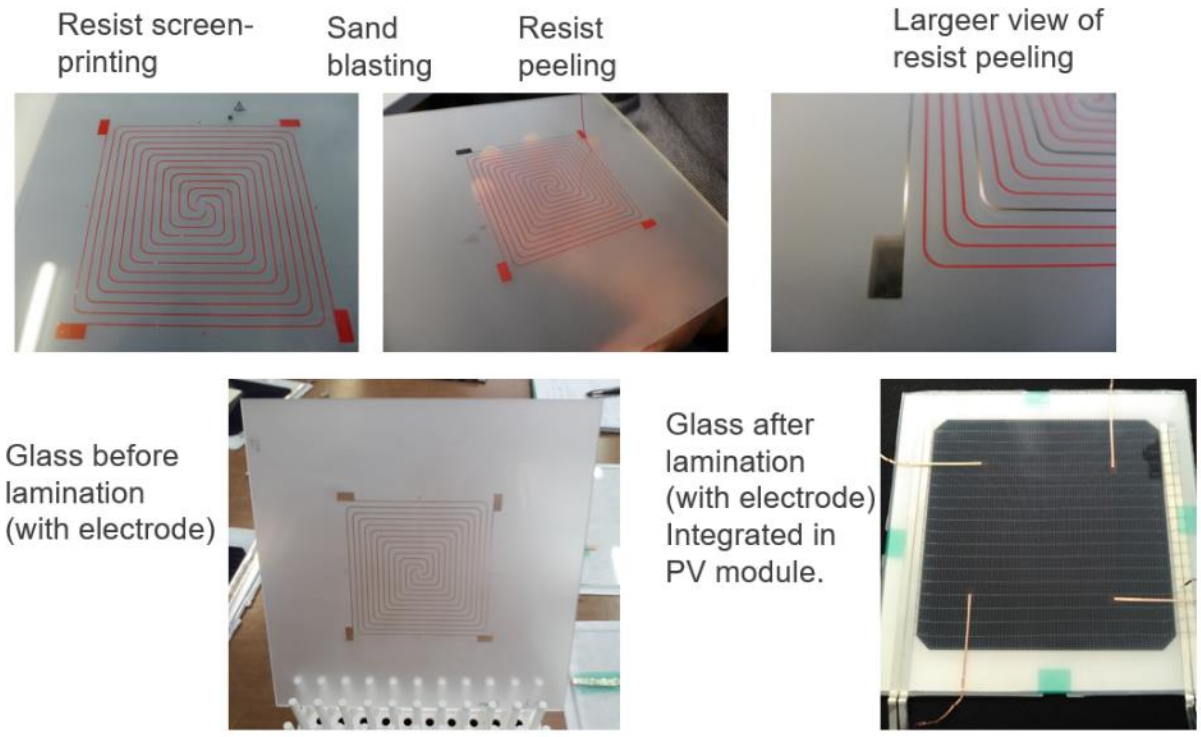

Fig. 3.4. Pictures of the process of spiral design fabrication using sand-blasting.

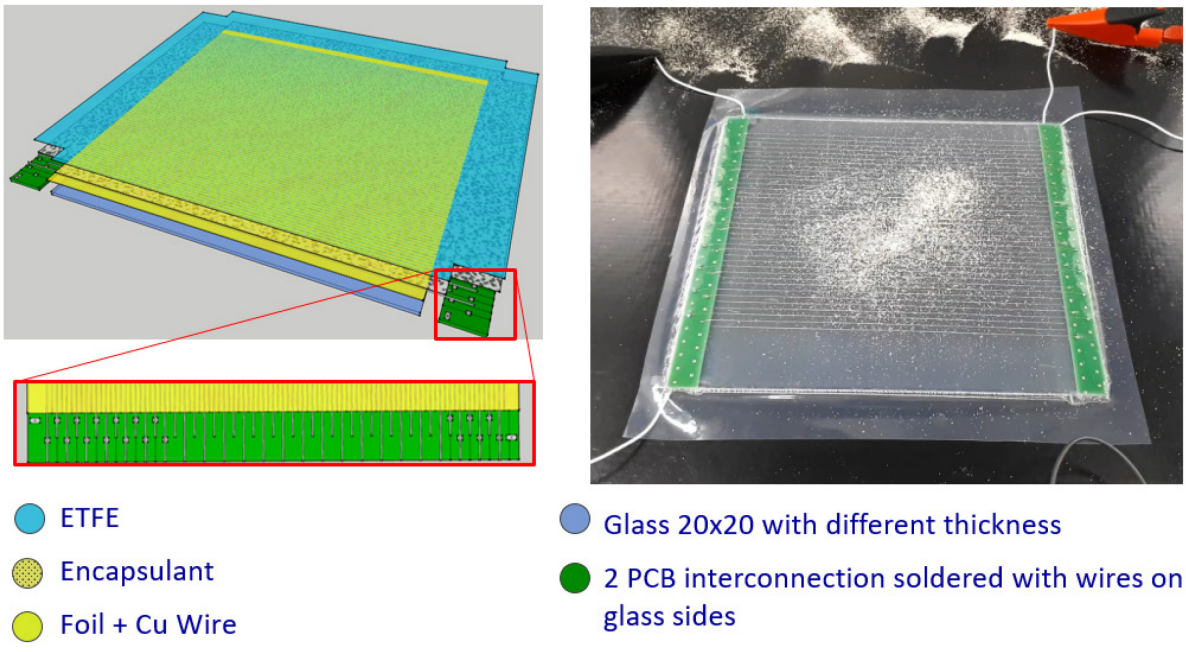

Fig. 3.5. Right: Scheme of the wire-electrode (WE) design and Left: pictures of the WE.

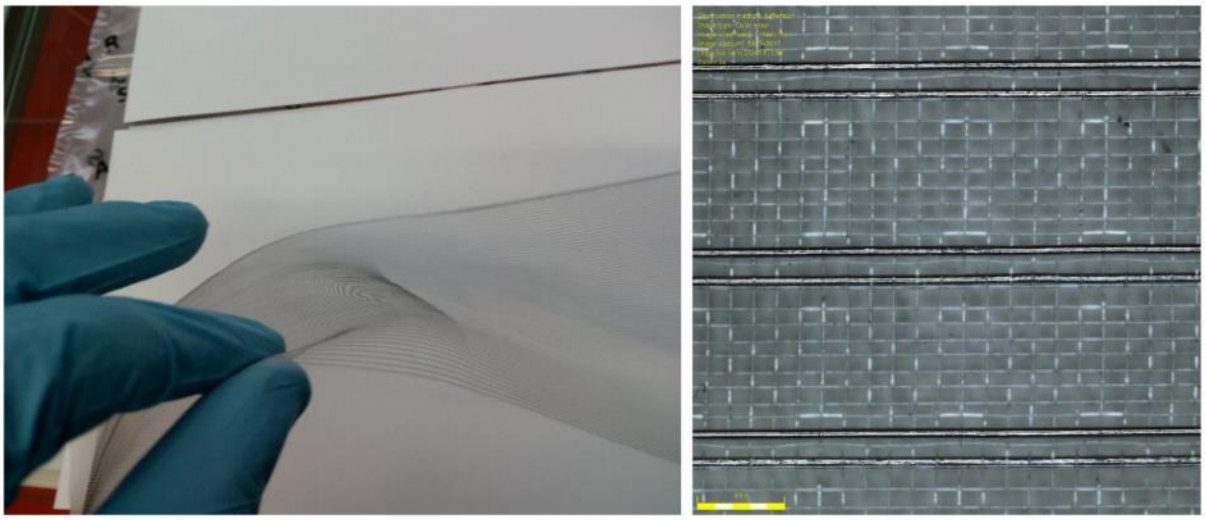

Fig. 3.6. Right: picture of the hybrid mesh from SEFAR and Left: images done with a digital microscope at a magnification of x10, the data-bar is equal to 1 mm.

2.2 Sample testing

Two different approaches were used to evaluate the cleaning efficiency of the fabricated samples. Static dust removal efficiency (s-DRE) and Output Power Restoration (OPR) [4]. In the case of s-DRE, the sand is distributed as homogeneously as possible on the sample surface before the EDS system is started and run for 60 sec. DRE equals $(1\text{-}m_f/m_i)$ with m_i the initial mass and m_f the final mass remaining on the sample active area (s-DRE approach simulates temporary activation of EDS system with accumulation of sand between electrodes' activation). Figure 3.7

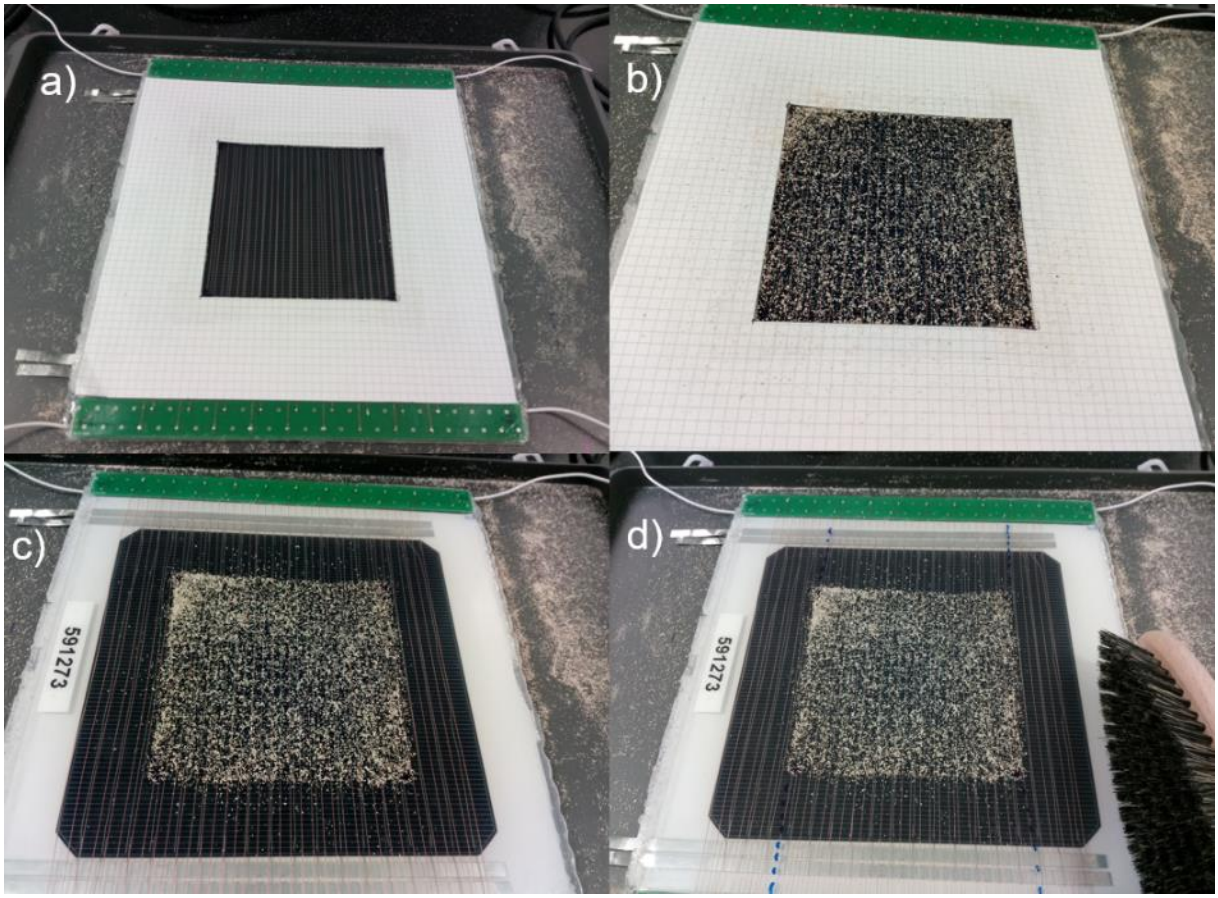

Figure 3.10. a) Sample with mask before dust deposition, b) sample with mask after dust deposition, c) sample without mask before testing, d) sample without mask after testing (low cleaning efficiency). The sand is weighted before putting on the module and after EDS cleaning (dust located inside the un-masked location).

Finally, OPR measures the short circuit current (Isc) of a single cell module with a surface of 156 cm^2 placed below the tested sample. The cell short circuit current (I_{SC}) is monitored during the full measurement (see Fig. 3.11), and OPR is defined as:

$$\mathrm{OPR}(\%) = \frac{I_f - I_{sand}}{I_0 - I_{sand}}$$

with I_0, the initial current without any sand at module surface, I_{sand} the current with the sand placed homogeneously on module surface, and I_f the final current after electrodynamic cleaning.

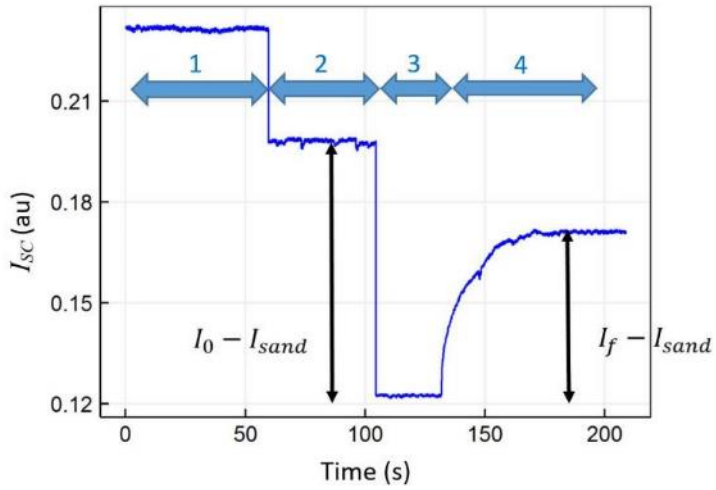

Fig. 3.11. Description of the current variation of the PV module during Output Power Recovery (OPR) procedure (period of time, 1: without EDS electrode, 2: with EDS electrode (I_0), 3: with EDS electrode and sand (I_{sand}) and 4: while cleaning using EDS, the stable current density is I_f).

2.3 New equipment: DustBuster

CSEM received the new equipment from CleanFizz called DustBuster. This equipment consists in a combination of two equipments: first a climatic chamber with controlled temperature, humidity and light and then a new high voltage pulse electronic charge with high flexibility of cleaning parameters.

2.3.1 DustBuster chamber

The chamber is composed of Aluminum and glass and equipped with a SIEMENS LOGO controller that can increase the humidity to a given value, turned on/off a light, blow sand using compressed air and controlled valve, turn on/off the electrodynamic cleaning system (see Fig. 3.12).
The goal of the chamber is first to make standard soiling cycles with repeated sequence to directly compare the effect of soiling on various samples. Secondly it can be used to simulate specific outdoor condition, for example the DustBuster can be directly connected to a climatic station in sandy region to mimic the weather condition of the specific site. The third use is the protection against high voltage, so the test can be run for long time without people controlling the machine.
The first task of CSEM was to control the equipment remotely from a computer. The control was done using VisualBasic in Excel as shown in Fig. 3.13a, all the functions F1: Light, F2: Humidifier, F2: sand injection and F4 for high voltage can be controlled from Excel. The output are also given in live in this control panel, with chamber temperature, chamber humidity, solar panel temperature and current output of the solar panel (see Fig. 3.13a). The second windows consist in a datalogger (Fig. 3.13b), for recording and visualization of the output parameters. The third window is for setting defined test sequences (Fig. 3.14).
Next DustBuster update should include an air dryer, a general chamber heater/cooler and a Peltier cooling system for heating/cooling the solar panel individually to reach the dew point for condensation

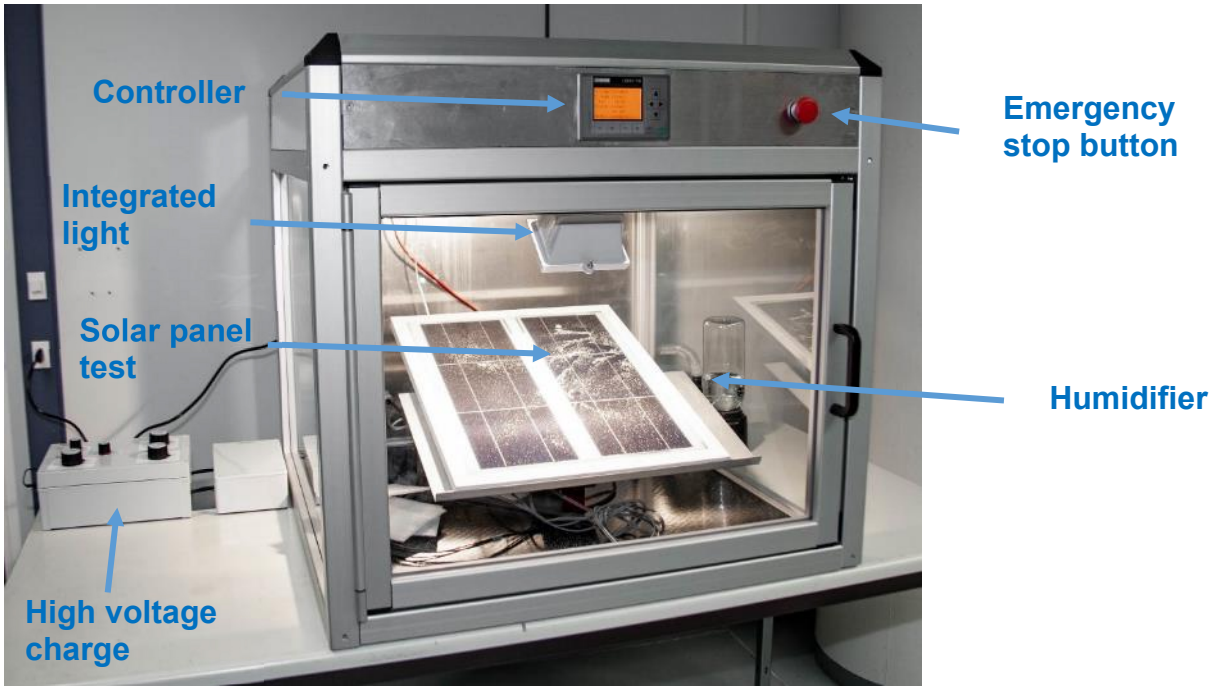

Fig. 3.12 DustBuster chamber composed of aluminum frame, security glass and controller.

(a)

CHAMBER "DUST BUSTER"

Loggo web server	
CONNECT	DISCONNECT

Dust Buster Chamber Monitoring	
BM Status:	Running
Chamber Temperature (AI4) [°C]:	24.2
Chamber Humidity (AI3) [%]:	63.0
PV Module Temperature (AI5) [°C]:	-50.0
PV Module Intensity (AI1) [A]:	1.1
Lamp (Q1):	ON
Humidifier (Q2):	ON
Sand Injection (Q3):	OFF
High Tension (Q4):	OFF
Time set:	#2018-11-29 13:51:15#

Dust Buster Chamber Control		
Lamp (F1)	F1 ON	F1 OFF
Humidifier (F2)	F2 ON	F2 OFF
Sand Injection (F3)	F3 ON	F3 OFF
High Tension (F4)	F4 ON	F4 OFF

(b)

"DUST BUSTER" DATA LOGGER

Data logger Control			
START	STOP	CLEAR DATA	SAVE DATA

Sampling time [hh:mm:ss]: 00:00:05
File Name: Test_Sequences_1

Chamber

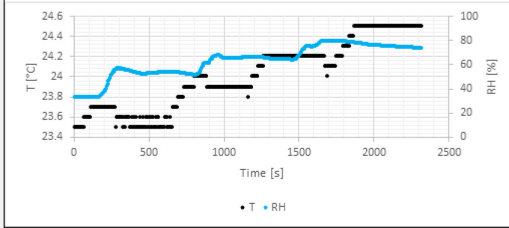

PV Panel

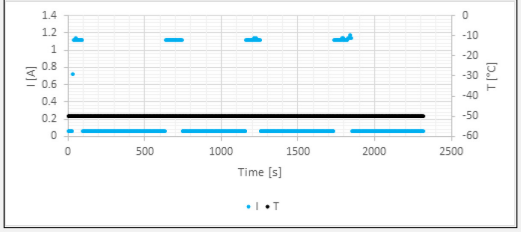

Fig. 3.13 DustBuster windows for (a) Monitoring and Control and (b) data logger

Sequence Control			
☑ Execute Sequence [Automatic Mode]			
Executing Step Information			
Current Step:	2		
Executing Code:	H 60		
Sequence Name:	Sequence1	SAVE SEQUENCE	LOAD SEQUENCE
Control Sequence			
1	S		
2	H 60		
3	W 200		
4	L 30		
5	F		
6			
7			
8			

Fig. 3.14 DustBuster window for sequence control for long soiling/cleaning test.

3 Results & Discussion

3.1 EDS optimisation

Electro-dynamic cleaning efficiency optimization depending on the electronics: like pulse frequency, phase shift and voltage was done on the new DustBuster (see Chapter 3). Only one sample used for these experiments is Sample 501273: ETFE/EVA/Cu300/EVA/PV-module of 20 by 20 cm^2.

Two different types of sand were tested in this study: a real Saudi Arabia sand (SAS) originating from King Abdullah University of Science and Technology (KAUST) area and a calibrated sand from Sibelco with specified particles dimensions of 0.2 to 0.5 mm. Optical images of the two sand varieties are given in Fig. 4.3, taken with an Olympus DSX100 opto-digital microscope, while further images were done with a Olympus LEXT microscope.

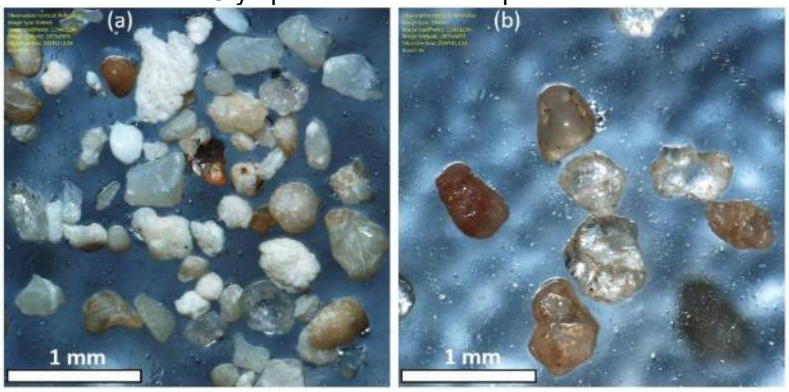

Fig. 4.3. Opto-digital microscopy image of the sand from (a) Saudi Arabia sand (SAS) from KAUST close to Jeddah and (b) calibrated Sibelco sand (0.2 – 0.5 mm).

The cleaning efficiency was measured for varying dust loading for the sample with wires and glass thickness (hf) of 1.03 mm covered by electronegative layer composed by a fluoropolymer. The observed trend is similar for both sand types, with a lower efficiency at low loading, with an optimum at intermediate loading and a decreased efficiency at high loading. The lower cleaning efficiency at high

sand loading is due to an accumulation of dust [20]. The pattern of sand accumulation changes for each test, the reason being the initial inhomogeneity of sand loading that creates accumulation as shown in Fig. 4.5. In these experiments, the current was injected in the photovoltaics mini-module to use it as an infra-red (IR) electroluminescence (EL) source. IR camera was used to take a picture every 6 seconds in order to observe the evolution of the cleaning during a static dust removal efficiency (s-DRE) test with average sand load of 320 g/m^2. The red circles in Fig. 4.5 highlight the inhomogeneity of initial sand loading. It is interesting to see that the locations where the loading is more important create some dust accumulations that will remain, in this case, until the end of the test. When the number of particles is too high, they start to stack and the electrostatic force cannot compensate anymore the force induced by gravity. Then only the particles close to the side of the accumulation can move. The representative dust loading density in the field will be much lower with about 0.1 g/m^2 per day in Doha as expressed by Guo and Javes [6]. As shown in Fig. 4.4, the cleaning efficiency at low dust loading is not optimal. This could be due to the lower interaction between particles that facilitate charge buildup of the particle surface by tribocharging [4].

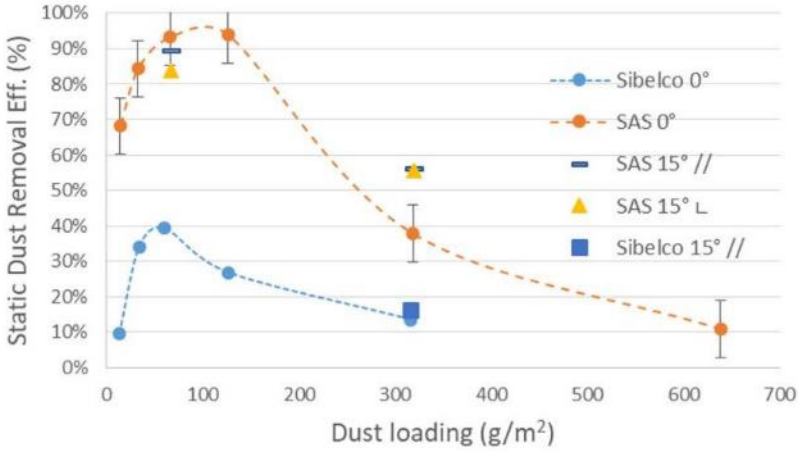

Fig. 4.4. Static dust removal efficiency versus sand or dust loading density for two different sands (SAS and Sibelco calibrated sand) on a sample with wires and glass thickness of 1.03 mm covered by additional layer (glass 1mm + ETFE). Samples are either horizontal or tilted by 15° for comparison with wire parallel (//) or perpendicular (∟) to the tilt axe. Lines are guides to the eyes.

When testing calibrated sand, the cleaning efficiency drops by more than 50%. The cleaning efficiency is known to have an optimum for particle size between 0.05 and 0.3 mm [5]. As the calibrated sand has particle between 0.2 and 0.5 mm, these different particles dimension are thought to be the reason for this lower cleaning efficiency. Particles size observed on solar panels are usually smaller than 0.2 mm in diameter [21, 22].

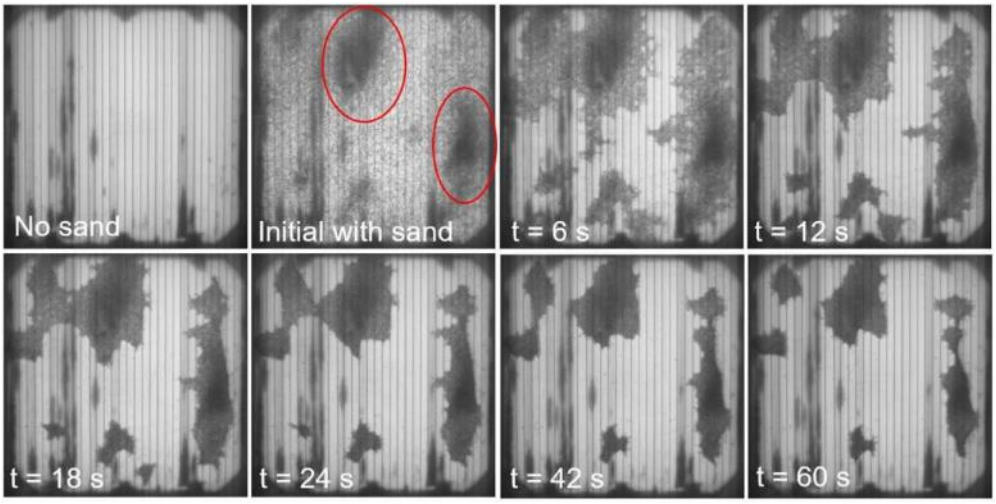

Fig. 4.5. Electroluminescence images before sand deposition, at initial stage and during static dust removal efficiency measurement. Average dust load density is 320 g/m^2. The red circles show the inhomogeneity of sand deposition with higher dust loading.

Tilting the modules at 15° improves the cleaning efficiency for SAS at high loading (320 g/m^2), without any effect of the orientation of the electrodes (perpendicular or parallel to the tilt axis). At loading below 100 g/m^2, a module tilt of 15° does not seem to have an effect on the cleaning.
In state-of-the-art electrodynamic systems, which can be found in the literature, the thickness of the glass or of the dielectric protective layer is typically found to be between 0.05 and 0.315 mm [4-6]), which is very interesting for cleaning efficiency but can bring to some limiting factors for reliability or for upscaling the electrodynamic device. In this experiment, the goal is to use affordable and more robust glass, which can finally be integrated in a front glass laminate of large area devices. Dedicated samples were fabricated with wire electrodes and varying cover glass thicknesses from 0.65 mm to 1.53 mm. For characterization, two different techniques were used to measure the cleaning efficiency at 0° tilt angle of the device under test and 320 g/m^2 sand loading density: cleaning efficiency (Fig. 4.6). A linear relation was observed between glass thickness and cleaning efficiency. Thinner glass improves cleaning efficiency but the quantitative results vary a lot, in particular for 0.6 mm glass the cleaning efficiency OPR is above 58%. One can see that for thick glass of 1.53 mm, the cleaning efficiency is of 22 % for OPR.
The outlier data point for a glass thickness of 1.2 mm is linked to a different sample composition: 1 mm thick glass, and 0.2 mm thick interface layer. The surface of the sample is composed of fluorine atoms, which is the most electronegative element. This high electronegativity induces a better positive charge transfer to the particles and improves the cleaning efficiency when the particles have a sufficient size [4]. If the particles are small and in contact to a highly electronegative surface, the Lewis acid-base force dominates and it is possible that small particles are then attached to the fluorinated surface [4].

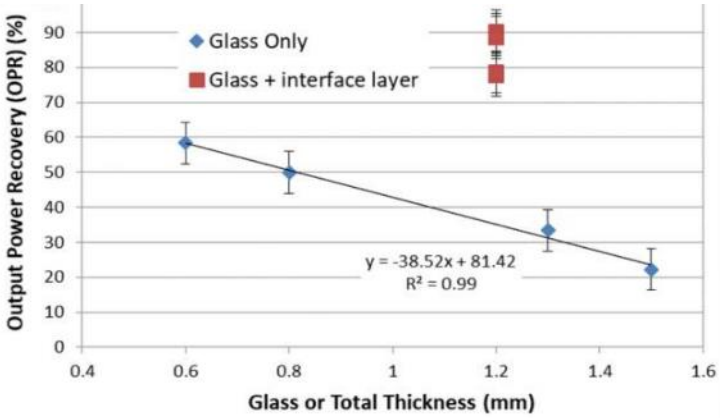

Fig. 4.6 Effect of glass thickness on cleaning efficiency (OPR). Tilt angle of the device under test equals to 0°.

3.2 Comparison of heating the PV module via the wire-electrode and via the PV cells

CleanFizz technology for cleaning the front surface of PV modules is based on creating electrostatic waves which swept away deposited dust. For the process to be efficient, the dust particles should not adhere strongly on the PV modules. It is well known that the presence of water increases the adhesion of the particles making more challenging their removal. At night time, air can be cooled to its dew point through contact with the colder PV surface, what results in condensed water on the surface of the modules. In order to avoid water condensation, the surface of the module can be heated. The aim of this study is to evaluate the feasibility of two different heating approaches to increase the surface temperature by 5 °C. The first one is to generate heat by means of an electrical current going through the CleanFizz wire electrodes, while in the second one, the current is to go directly through the solar cells to heat the module surface.

3.2.1 Simulation

Both approaches have been modelled by means of the finite element method, using the commercial software Comsol Multiphysics.

3.2.2 Heating through wire electrodes

In order to calculate the temperature at the front surface of the module, a 2D model has been used. The geometry of the model, as well as materials, and boundary conditions are shown in figure 4.8. In the model, the wire electrodes are separated (P) 8 mm and they are situated (h) 0.55 mm below the front surface of the module. The heat enters inside the domain through these wires. They are considered perfectly cylindrical, with a diameter (d) of 35 μm, and made of stainless-steel. The measured electrical resistance for each wire is 9 Ω/cm. In a single cell module, their length (L) is to be 20 cm. Thus, the resistance (R) for each wire is 180 Ω. When an electrical current (I) circulates through the wire, the dissipated power (P) can be calculated using the following equation:

$$P = R.I^2$$

And the heat influx (HI) through the wire can be estimated from:

$$HI = \frac{P}{A_{wire}} = \frac{R.I^2}{2.\pi.\left(\frac{d}{2}\right).L}$$

For the first simulation, a current of 25 mA is going through the wire generating a heat influx of 5116 $W.m^{-2}$.

Once discussed how the heat influx is estimated as a function of the current, next point is to determine how the PV module exchange heat with the surroundings. Here, it is assumed that heat is exchanged with the medium by radiation. The top and bottom surfaces of the module radiate energy towards a medium which is considered to be at 20°C. Thus, cooling by convection due to wind is not taken into account.

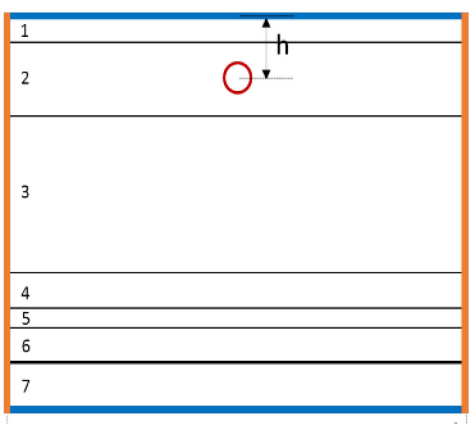

Heat Influx
No heat transfer
Radiation exchange condition (T_{amb} = 20°C)

Domain	Material	Heat capacity C_p [$J.Kg^{-1}.K^{-1}$]	Thermal conductivity K [$W.m^{-1}.k^{-1}$]	Density ρ [$Kg.m^{-3}$]	Emissivity
1	ETFE	1000	0.24	1800	0.89
2	EVA	2090	0.311	950	-
3	Glass	2090	0.311	950	-
4	EVA	2090	0.311	950	-
5	Cell	677	130	2330	-
6	EVA	2090	0.311	950	-
7	Back-sheet	1250	0.15	1200	0.9

Figure 4.8. Scheme of the model used with defined geometry, boundary conditions and thermal properties of the materials.

The model was run with the previous assumptions and the main results are summarized in figure 2. The PV module starts heating from 20 °C. After 20 minutes, the temperature of the module increases up to 25 °C. The module temperature continues rising up to 27.18°C where it reaches an equilibrium with the medium and stabilizes. The temperature at the top surface of the module is not spatially uniform. Above a wire, the surface temperature is 0.55 °C higher than a point placed between two wires.
Form this simulation, it can be stated that the temperature of a single cell PV module consisting of 25 heating wires can be increased from 20 °C up to 27.18 °C and kept at this level during 3 hours by using an energy of 8.44 Watt hour.

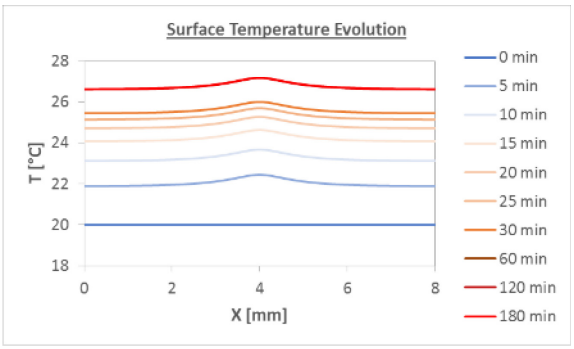

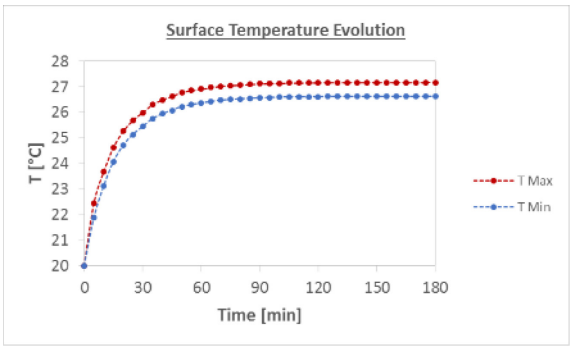

Figure 4.9. Modelled surface temperature when heating through wires at different time steps (A). Maximum and minimum temperatures at the module surface as function of the heating time (B).

3.2.3 Heating through the solar cell

In order to simulate the heating of the PV module through the solar cell, the previous model has been modified as shown in figure 3 (A). In that case, the heat influx comes from the top and bottom surface

of the solar cell. In order to estimate the heat influx, the following equation which relates the voltage of the solar cell (V) with the current (I) is used.

$$V = \frac{n.K.T}{q}.\ln\left(\frac{I}{I_0}\right)$$

Where n is the ideality factor, K the Boltzmann constant, T the junction temperature, q the electron charge and I_0 the dark saturation current. Table I summarizes the values used in our calculation. Once the current and voltage specified, the heating power of the cell is calculated as its product. The heating influx is determined as the heating power divided by the area of the cell, in our case, 0.049 m^2. For this first simulation, a current of 4 A has been selected resulting in a heat influx of 52 W/m^2. Half of this flux entering from the top surface of the cell and the other half from the bottom.

Parameter	Value
n	1
K [m^2 kg s^{-2} K^{-1}]	1.38E-23
T [°C]	28
Q [C]	1.6E-19
I_0 [A]	1E-10

Table 4.1. Parameters used in the solar cell model.

A part from the heat influx, the rest of the model is equivalent to the one presented by the heating through the wire, i.e. materials and heat exchange towards the surrounding kept at 20°C by radiation. The model was run and the main results are summarized in figure 4.10 (B). The top and bottom surface of the module stabilizes to a temperature close to 25 °C. The bottom surface reaches this temperature after 35 minutes while the top surface after 95 minutes.

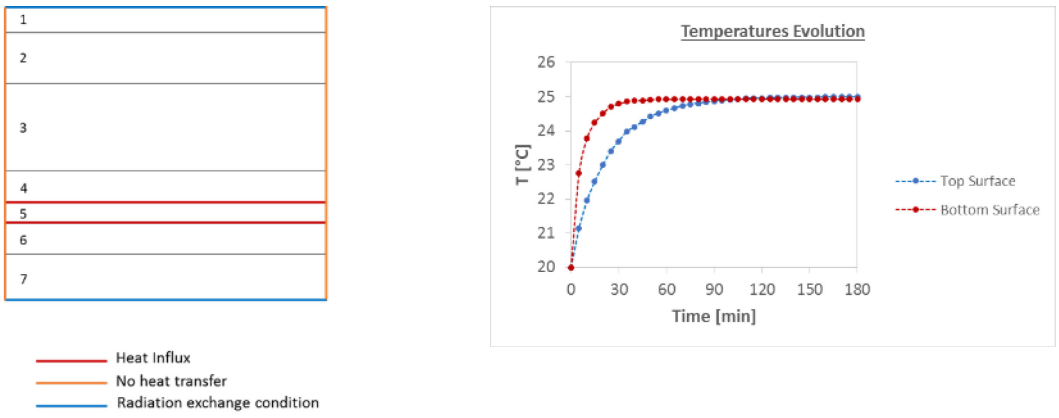

Figure 4.10. Scheme of the model used with defined geometry and boundary conditions when heating through the solar cell (A). Temperatures at the top and bottom surface of the module as function of the heating time (B).

From this simulation, it can be stated that the temperature of a single cell PV module can be increased from 20 °C up to 25 °C and kept at this level during 3 hours by using an energy of 7.59 Watt hour. In that case we use less energy than heating through the wires but also the final temperature is lower. In order to have a better comparison between the two approaches, the current passing through the cell has been modified to a value of 5.75 A. The results obtained for this case are compared to the results obtained when heating through the wires (see figure 4.11). For both cases, a stabilized temperature of 27.18 °C is reached. However, when heating through the cell during 3 hours, an energy of 11.1 Watt hour is required, while when heating through the wires, the energy required was 8.44 Watt hour. Thus, in order to reach and keep the same temperature of 27.18°C, when heating through the solar cell it cost

31% more energy than heating though the wires. Moreover, the final temperature is also reached faster when heating through the wires.

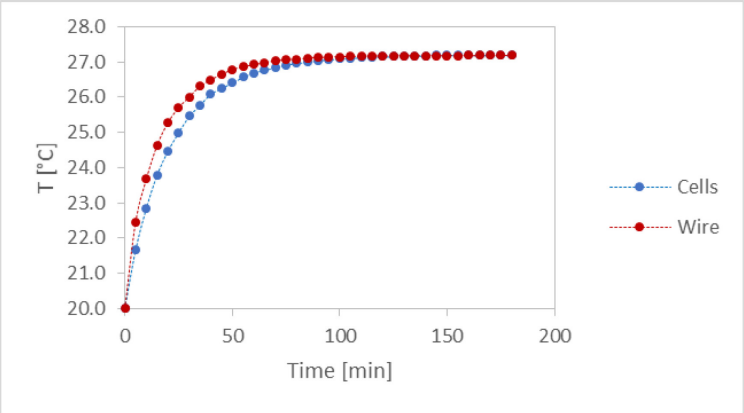

Figure 4.11. Comparison between the temperatures measured at the top surface of the module when heating either through the cell or through the wire to reach an equivalent final temperature of 27.18°C.

3.2.4 Experiment

An experiment to increase the temperature of a single cell module has been carried out by heating, first through the wires, and then through the cell. When heating through the wires, the temperature of the module has been increased from room temperature up to 32.5 °C in 10 minutes. A thermal image of the heated module is shown in figure 4.12 (A). The module consisted of 46 wires and a current of 21.7 mA was passing through each wire during heating. The power supply used during the heating was delivering 5.2 W. After this 10 minutes, the heating was stopped and the module cooled down. The temperature was monitored during the whole cycle and it is shown in figure 4.13 (A). The full process has also been simulated with Comsol. As can be seen in figure 4.13 (A), the calculated values for the temperature follow closely the measured ones.

On a second step, the first module was heated through the solar cell. Equivalently, the temperature of the module was increased up to 32.3 °C. The final temperature was reached after 13 minutes. A thermal image of the module is shown in figure 5 (B) after 10 minutes of heating. In that case, during the heating the power supply was delivering a current of 4 A, and a power of 3.6 W. After 13 minutes, the power was turned off and the module let to cool down. The temperature measured during the whole cycle is shown in figure 6 (B). As in the previous case, the full cycle has been seen simulated with Comsol and, as can be seen in figure 6 (B), the calculated values for the temperature follow the measured ones.

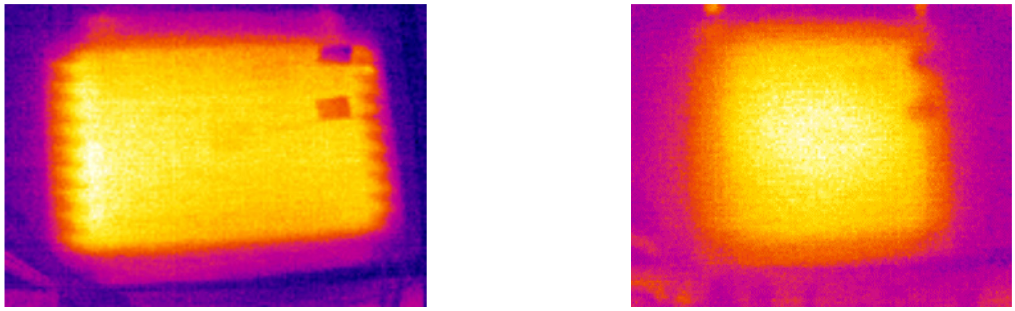

Figure 4.12. Thermal image of the sample after 10 minutes of heating through the wires (A) and through the cell (B).

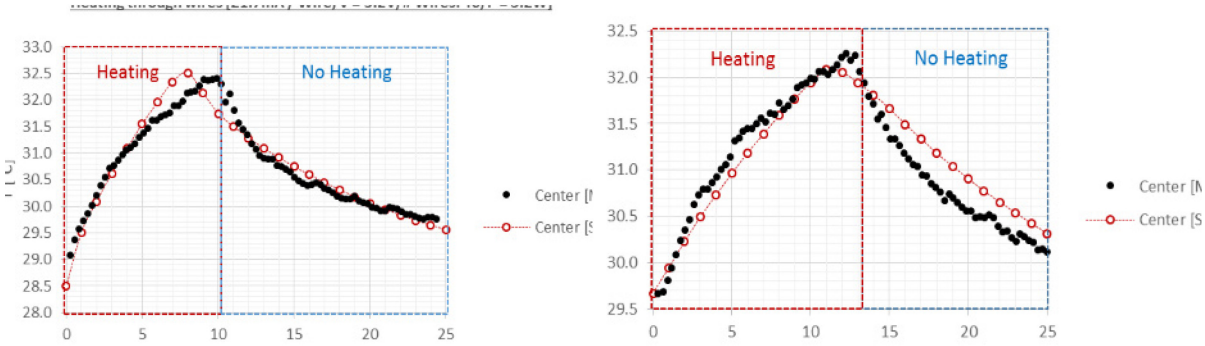

Figure 4.13. Comparison between model and measured data

3.2.5 Conclusions of heating via wire electrode

3.3 Simulation of Electro-dynamic Cleaning System (EDS)

To help us understanding what is the major parameters influencing the cleaning efficiency of EDS, modelling is done first for electric field at the surface of the sample and secondly for dust particles movement.

3.3.1 Dust Particles Trajectory Calculation

This sub-chapter is a pre-study to try to simulate the particles trajectory on EDS surface depending on the charge number, charge polarity, particles size and frequency. The approach solves 2nd Newton's Law for charged particles [4]:

(1) Particle in Air → Electric Force (qE) + Gravity (mg) + Stokes Drag $(D = 6\pi\eta r_{particle}^2)$

$$\begin{cases} m\ddot{x} = qE_x - D\dot{x} \\ m\ddot{y} = qE_y - D\dot{y} - mg \end{cases}$$

(2) Particle on **EDS Surface** → Electric Force (qE) + Gravity (mg) + Stokes Drag + Sliding Friction $(\mu N = \mu * (mg + F_{adh} - qE_y))$ + Adhesion Forces (F_{adh})

$$\begin{cases} m\ddot{x} = qE_x - D\dot{x} - \mu N \\ m\ddot{y} = qE_y - D\dot{y} - mg - F_{adh} \end{cases}$$

The Adhesion forces can be Van der Waals force (F_{vdw}) for distance-dependent interactions between atoms and molecules produced by momentary movements of electrons and capillary force (F_{cap}) Important when on the surface of the EDS a thin film layer of water is present.

$$F_{vdw} = \frac{H d_{particle}}{12 * s^2}$$

- H → Hamaker constant (10^{-18}-10^{-19} J)
- $d_{particle}$ → Particle diameter.
- s → Particle-surface distance.

$$F_{cap} = 4\pi * \gamma_{water} * r_{particle}$$

- γ_{water} → Surface tension for water (76 mN/m)
- $r_{particle}$ → Particle radius.

Procedure Calculate Electric force for a dust particle placed on the Electrodynamic Screen (refer figure 4.19):

1) Identify voltage signal applied on each electrode (i.e. periodic squared signal; Period (T))
2) Define phase shift between the signals applied on neighboring electrodes (i.e. 120°)
3) Identify different voltage configurations occurring (i.e. 6 different sections)
4) Calculate electric field for each different configuration taking into account geometry and boundary conditions (Finite Element Method; FEM).
5) Use periodicity to determine electric field distribution (E) as function of time (t) and position (x): *E(t,x) = E[ceil(n_sections*mod(t,T)/T),mod(x,Tx)]*
6) Calculate Electric Force on dust particle: *q*E(t,x)*

Matlab® graphical user interface (GUI) was used to implement the particles trajectory calculation and results presentation (see figure 4.20).

Sensitivity study of the particles charge trajectory is presented in figure 4.21 and Table 4.2. The particles can move in diverse mode, the first is the hoping mode and the second, the sliding mode. Then the direction of movement can be always the same or the particles can be in alternating mode with forward and backward movement and without net displacement.

The first interesting point in table 4.2 is that changing the charge polarity does not change the direction of movement but changing the particles size with the same charge polarity and absolute value can change the moving direction.

Small particles are moving in hoping mode always in the same direction, larger particles are moving in sliding mode always in the same direction, even larger particles are then moving is sliding mode in alternating direction (forward and backward direction), then the largest particles are not moving anymore.

By reducing the absolute charge of a small particles, it has the same effect than having larger particles with larger absolute charge (reducing the charge from 3.5E-15 C to 1E-15 C for 10 microns particles make the same effect that having same charge 3.5E-15 C but having particles radius of 40 microns).

By reducing the frequency from 15 to 10 Hz, the particles of same size with similar absolute electric charge can move better (particles with 10 microns in radius is alternating at 15 Hz but it is sliding forward at 10 Hz).

This sensitivity study shows that to have an efficient cleaning electro-dynamic system (EDS) it is important to have a sweeping mode of frequency to find the right frequency for each particles size and charge to be moved always. It is also important to have a good charging process for particle this could be done by applying a constant high voltage charge to the electrode (positive or negative) or to have a surface layer with high electronegative or electropositive element at the surface. This will have the possibility better transfer charges from the surface to the particle. This was demonstrated experimentally in chapter 4.1 by changing the top layer from glass to fluoro-polymer, the fluor has the highest electronegativity of the periodic table then this element will attract electron and will induce positively charged particles.

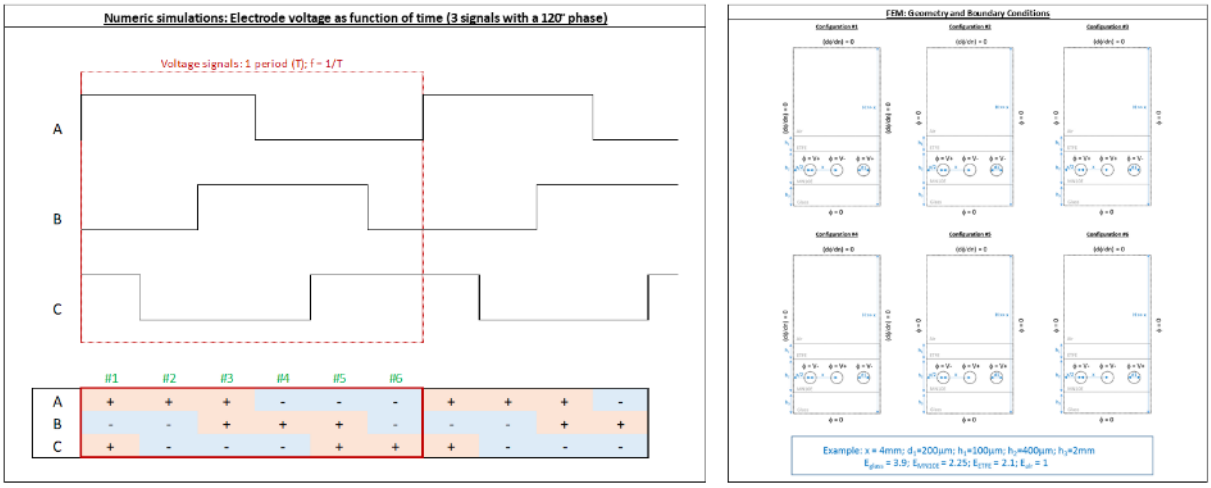

Fig. 4.19 Sequence of the EDS signal and electrode voltage as function of time

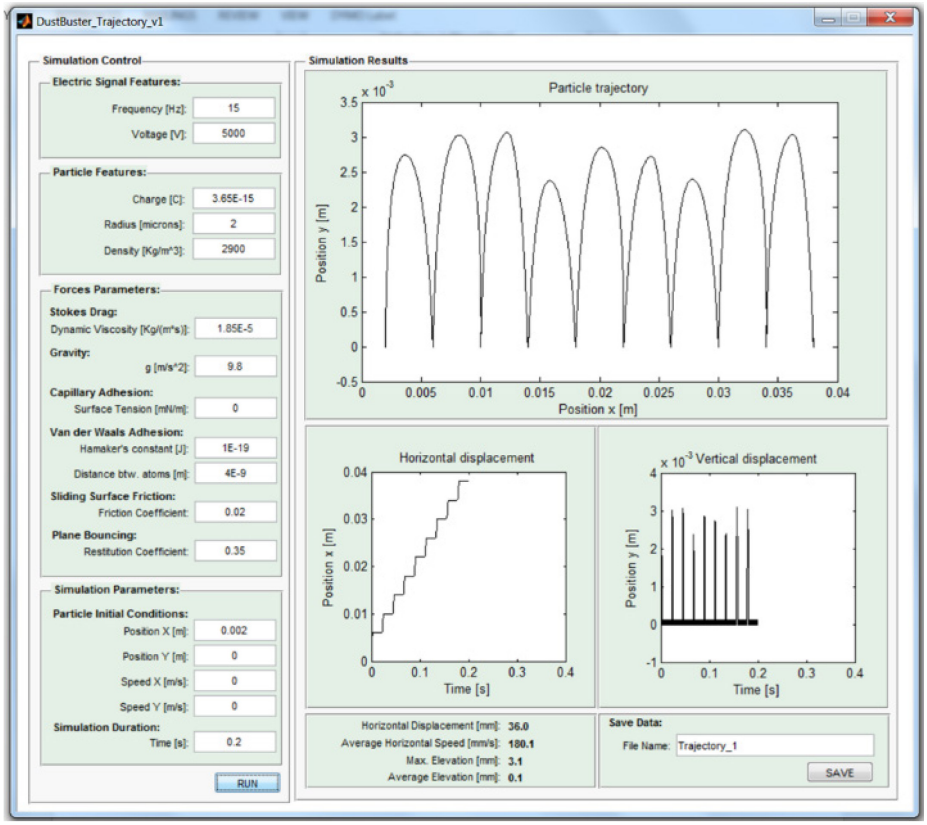

Fig. 4.20 Matlab GUI designed to estimate the trajectory of a charged particle.

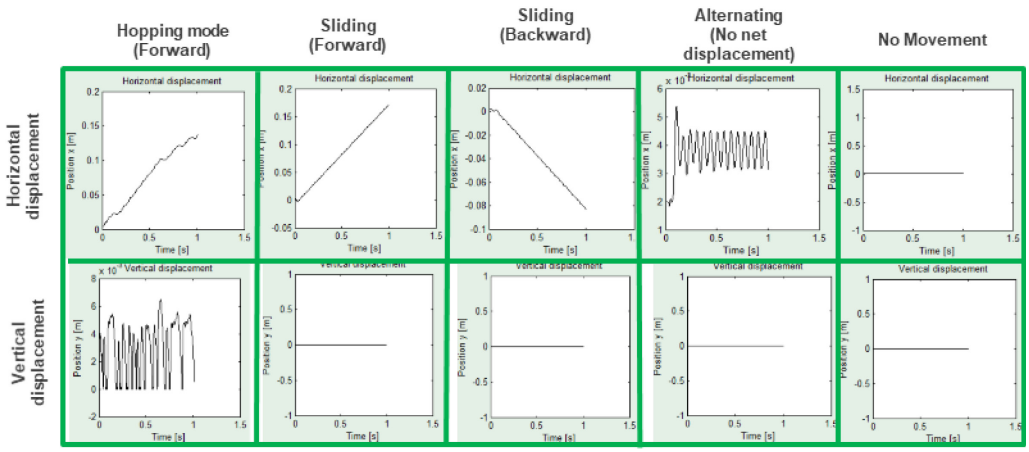

Fig. 4.21 Horizontal and vertical displacement for the different moving description from table 4.2

Table 4.2 Particles movement depending on EDS parameters and the particles radius and charge.

Freq. [Hz]	V [V]	Radius [μm]	Charge (C)	X_0 [mm]	Description
15	5000	10	3.46E-15	2	Particle moves forward in hopping mode.
15	5000	10	-3.46E-15	2	Particle moves forward in hopping mode.
15	5000	20	3.46E-15	2	Particle moves forwards sliding on the surface.
15	5000	35	3.46E-15	2	Particle moves backwards sliding on the surface.
15	5000	40	3.46E-15	2	Particle moves forward and backward alternatively (No net displacement).
15	5000	50	3.46E-15	2	No movement.
15	5000	10	1E-15	2	Particle moves forward and backward alternatively (No net displacement).
10	5000	10	1E-15	2	Particle moves forward sliding on the surface

Particle density (Si) = 2900 Kg/m^3 / Van der Waal's (H = 1E-19 J / s = 4E-9 m) / No capillary adhesion force / Sliding friction coefficient t= 0.02 / Restitution coefficient: 0.35 / Dynamic viscosity air (Stokes Drag): 1.85E-5 Kg/m·s

3.4 Up-scaling of the wire-electrode

This topic was one of the major goals of the project and indeed it was also a challenging task. On small sample of about 15 by 20 cm2 (one cell module) the yield of production was very good. When passing at 40x40 cm2 meaning about 5 times larger surface. Over 10 large samples were not working whereas the small sample were all working. After deeper inspection of the sample the shunts could be observed as shown in Figure 4.22 and revealed that some dust of hair could be the cause of the non-working samples. Based on these observation, cleaner environment and specific encapsulant cleaning process were put in place. These changes improved a lot the fabrication yield of sample.

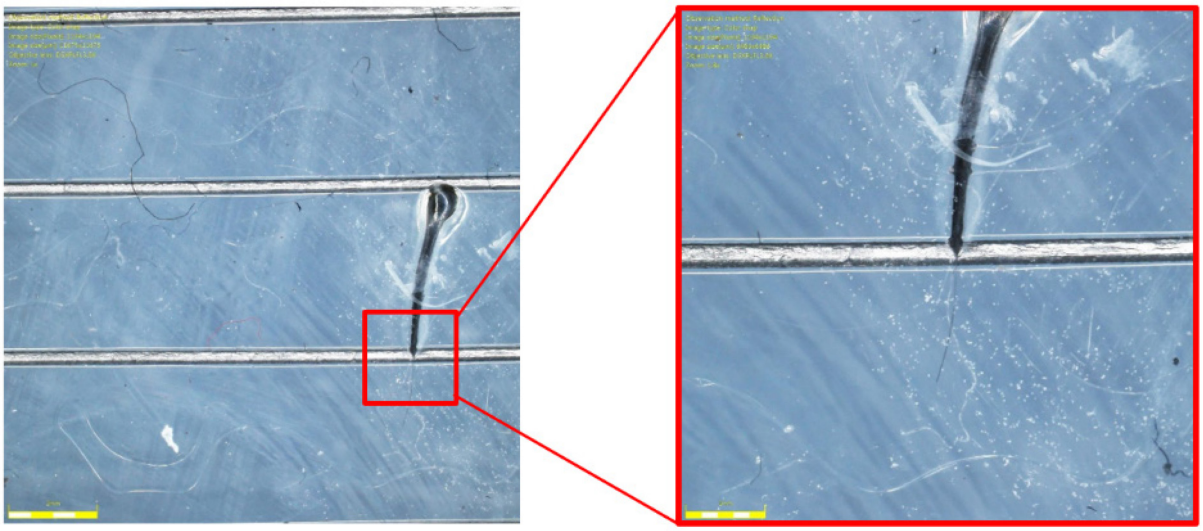

Fig. 4.22 Optical microscopy imaging of a shunted sample (right) at medium zoom and (left) at higher zoom.

The first implementation was done with ETFE front sheet and PBC with only two polarities contact. The ETFE enable to have high cleaning performance and remove some shunted area before the optimized process were implemented (see Fig. 4.23 right). With the PCB with only two polarities per side the wires are not hold on both sides which make the wire swimming in the sample (see Fig. 4.23 left). With the PCB with 4 connections on both sides the wires stay straight.

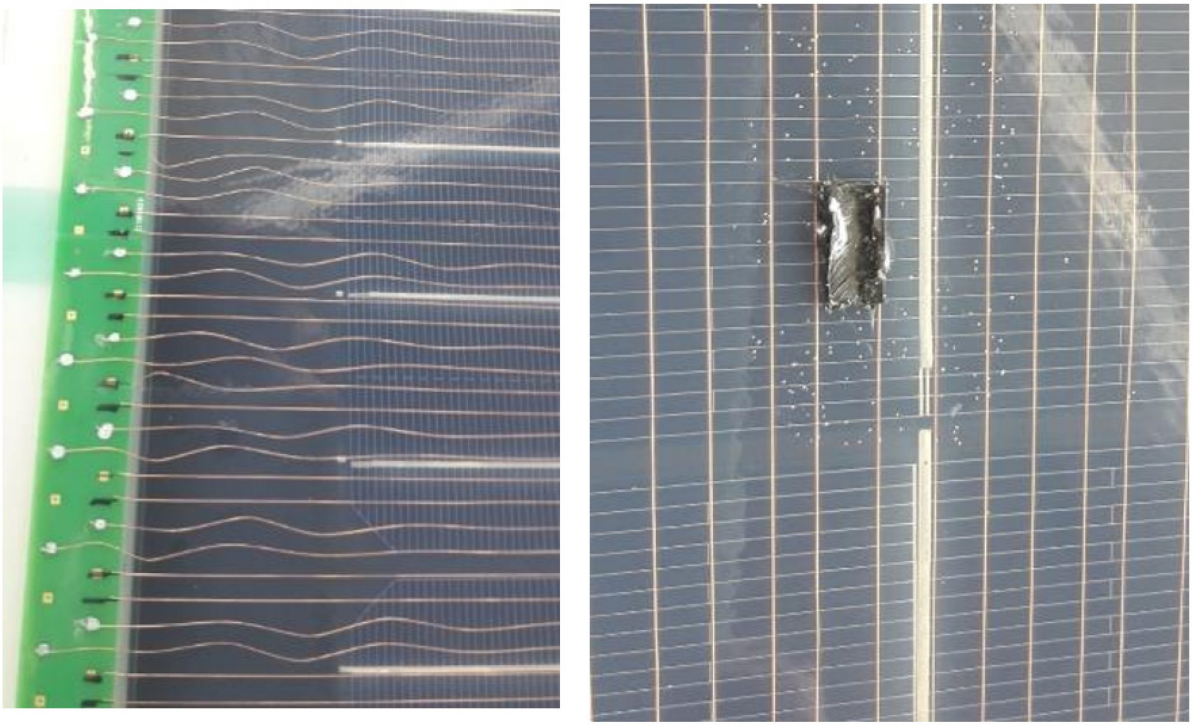

Fig. 4.23 Images of (left) the swimming of the wire due to only one side attachment and (right) repaired shunt between to electrode wire.

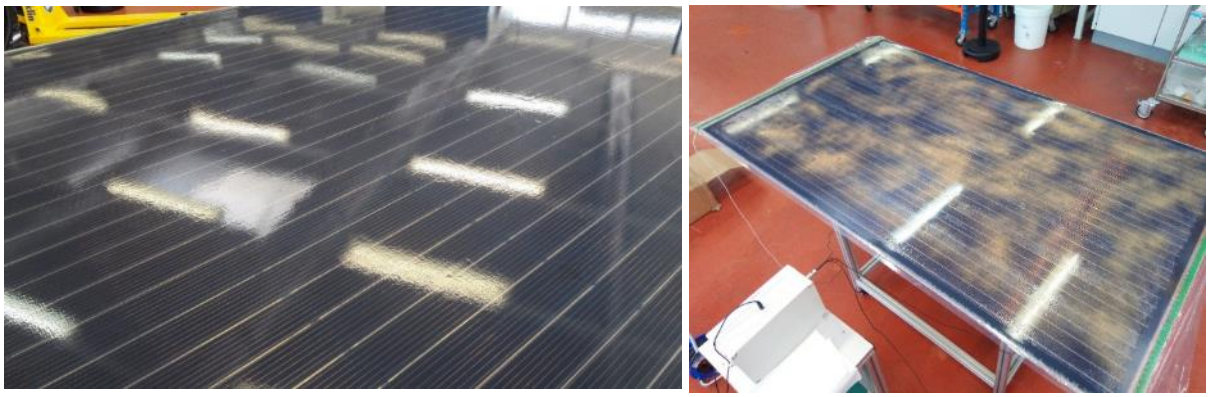

Fig. 4.23bis. (Left) Picture of EDS integrated in a standard PV module (zoomed view) (right) Picture of the full PV module with EDS wire-electrode electrode with dust on it.

3.5 Cost Calculation of Electro-dynamic Cleaning System (EDS)

In this sub-chapter, calculation is done for cleaning cost saving of PV installation based on outdoor test of PV system including EDS cleaning technology compared to reference PV system. The second part of this sub-chapter reports cost calculation of EDS electrode production.

3.5.1 Outdoor field test of EDS

CleanFizz has been conducting first outdoor tests of EDS performances on PV modules at KAUST (King Abdullah University for Science and Technology) near Jeddah in Saudi Arabia, since March 2015. The performance of the modules is assessed by monitoring the modules ISC every minute. The ambient temperature, the panel surface temperature and the humidity are monitored as well. The pilot test is remotely controlled by CleanFizz and the collected data is transferred on a daily basis to a server in Geneva, Switzerland.

The setup consists of four identical PV panels of 40x50 cm^2, mounted on a tracker structure equipped with an actuator for vertical rotation, the tilt angle being fixed to 30° (Fig. 4.25). Two PV panels are connected in series and have the electrodynamic cleaning system (EDS) connected and activated by the electronics every 4 hours for 3 min (6 sessions of EDS per day) while the other two reference panels are monitored without EDS (also connected in series). The electrodes have spiral design based on patterned and etched transparent conductive oxide (TCO). After a certain period of time and data collection, all modules are cleaned manually at once.

To reduce measurement noise from the monitoring results, integrals of the ISC over time were calculated for both cleaned and uncleaned modules. Both the measured ISC and its integral were then compared between the EDS modules and the reference modules.

Fig. 4.25. Pilot field test of the electrodynamic cleaning system (EDS) from CleanFIZZ at KAUST (King Abdullah University for Science and Technology) near Jeddah in Saudi Arabia.

3.5.2 Field data of electrodynamic cleaning system (EDS)

The field test system installed at KAUST is equipped with humidity and temperature sensors and records short circuit of both reference and electrostatically cleaned modules. At night, the panel temperature is lower than exterior temperature due to radiation of the solar panel (Fig. 4.26). The lower temperature of the module surface can induce water condensation at the panel surface when the dew temperature difference with panel temperature is smaller than 5 K. The condensed water can strongly attach dust to the glass surface via cementation [24].
Fig. 4.27 shows the evolution of the atmospheric measurements during each month from the monitoring start in March 2015 to the end of 2017. Missing months indicate data recording interruption. Overall relative humidity changes from about 35% during the day to more than 75% at night, depending on seasonal variation. Module temperature varies over 30 K, from 20°C at night to a maximum of 50°C at noon.

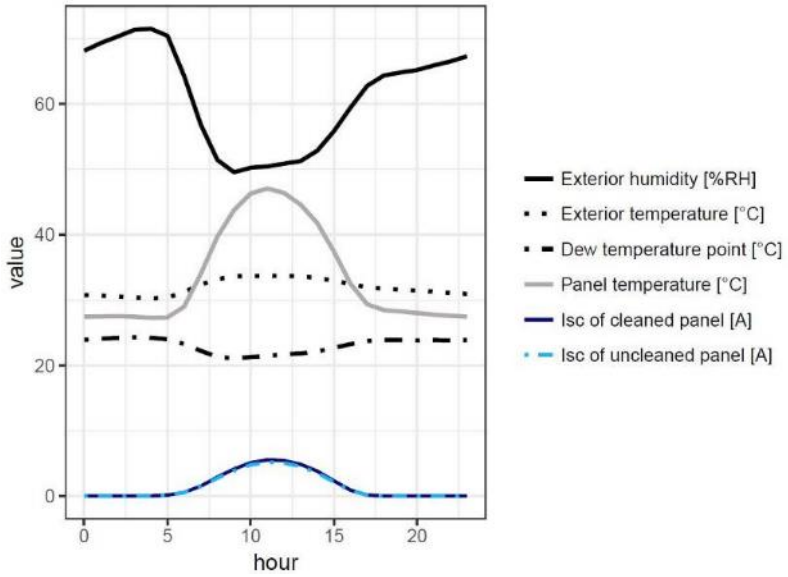

Fig. 4.26 Average of daily atmospheric data and module I_{sc} of the full year 2015.

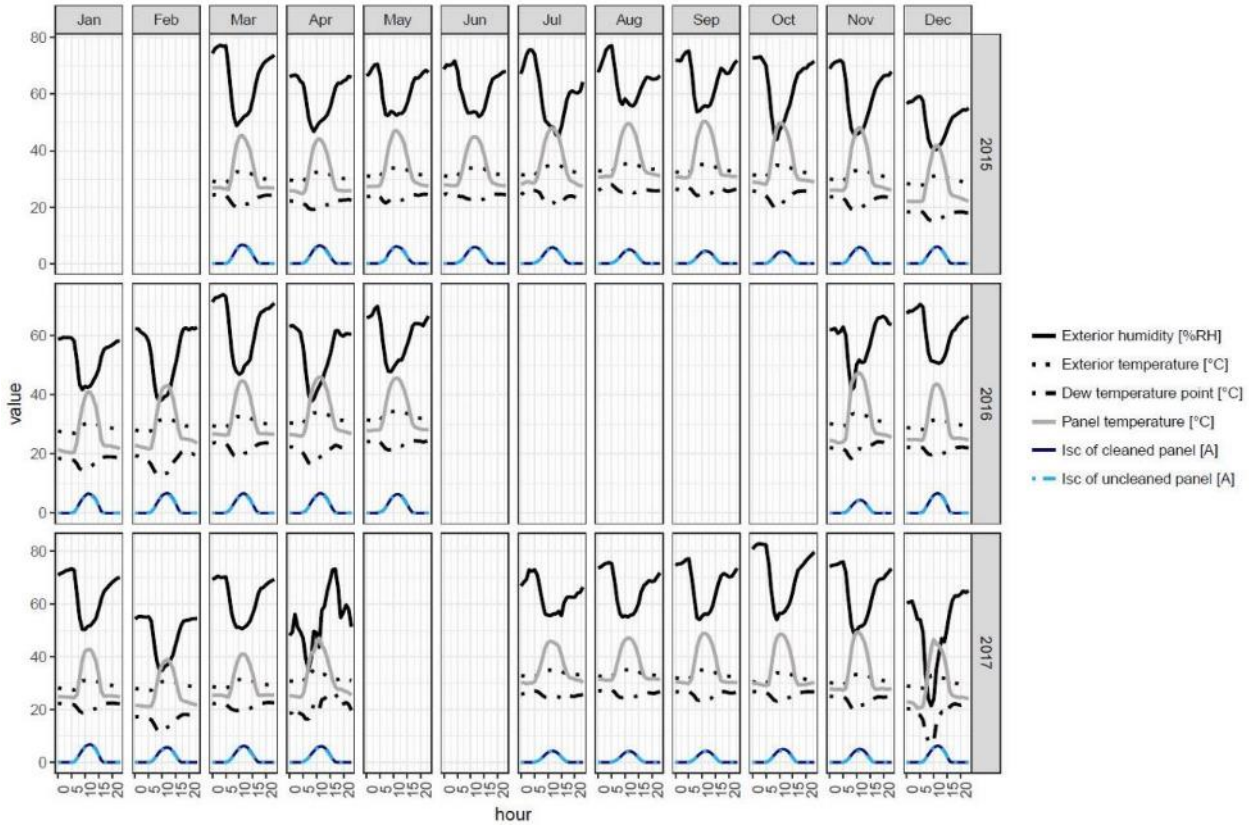

Fig. 4.27 Average of daily atmospheric data and module I_{sc} over each month from 2015 to 2017.

The short circuit current of both reference module without cleaning (blue line) and module with electrodynamic cleaning (red line) are shown in Fig. 4.28 Some manual cleaning can already be highlighted: For instance, I_{SC} values strongly increase in November 2015, which corresponds to a reset of I_{SC} after washing both solar modules (reference and with CleanFizz electrode). Another cleaning can be identified when the measurements restart end of November 2017. All five cleaning sessions are

indicated with a vertical line and noted from C1 to C5 on Fig. 4.28. This graph also highlights the periods with missing data recording from May to November 2016 and from March to July 2017. The 6 periods during which the evaluation of current will be studied are the following:
P1. 1st March to 1st May 2015 which corresponds to the start of measurements.
P2. 20th June to 11th November 2015, allowing to examine the evolution after the first cleaning.
P3. 1st January to 20th February 2016, covering the beginning of 2016 until the third cleaning.
P4. 22nd February to 18th April 2016, which are the relevant data before interruption of data recording.
P5. 30th November 2016 to 20th March 2017, which is the period on measurements resumption.
P6. 9th October to 15th November 2017, which are the only periods with data recording in 2017.

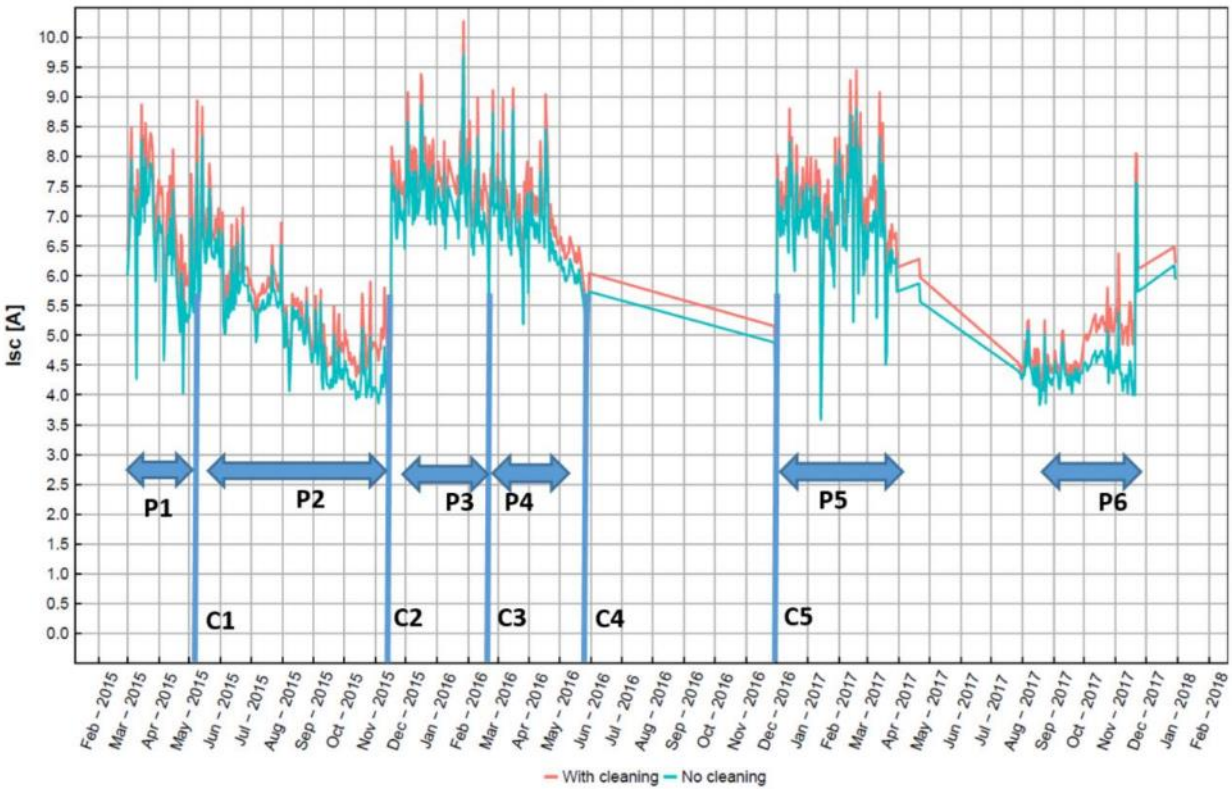

Fig. 4.28 Maximal short-circuit current for each day ($I_{sc(max)}$) measured from March 2015 to December 2017. Blue line corresponds to the reference PV panels without the cleaning system while the red line is for the PV panels equipped with the electrostatic wave cleaning technology. Five manual cleaning dates and six studied periods are noted from C1 to C5 and from P1 to P6, respectively.

To reduce the measurement noise and to be closer to the daily produced energy, the I_{SC} is integrated over each day, as shown in Fig. 4.29a and 4.29c. It is assumed that the loss in open circuit voltage (V_{OC}) due to soiling (lower irradiance induces lower injection and lower V_{OC}) is compensated by an increase in fill factor (FF) (at lower irradiance, the loss in series resistance is reduced increasing FF). For confirmation, a similar module was measured at 450 W/m^2 (compared to 1000 W/m^2) and the relative difference in V_{OC}*FF product was less than 0.5% compared to the value at 1 sun. Taking the V_{OC}*FF product as a constant with respect to the soiling losses (in this study the irradiance varied between 0.55 and 1 sun), the power is then directly proportional to I_{SC}, meaning that the daily energy production is proportional to the time integral of I_{SC} over the day. With this assumption, the relative loss of daily energy due to soiling is in a first approximation relatively equivalent to the relative loss of daily integral of I_{SC} due to soiling.

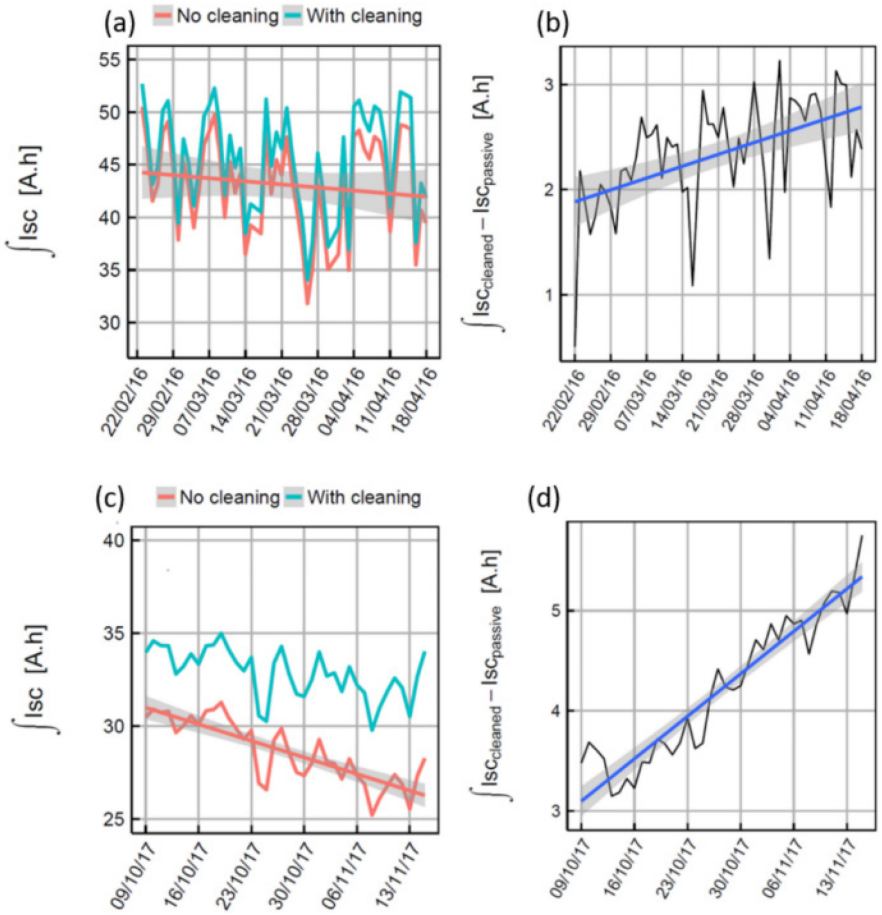

Fig. 4.29. Integral of current density over each day for electrodynamic cleaned panel (in light blue) and reference panel (in orange) for (a) period 4 and (c) period 6. Difference of both panels over (b) Period 4 and (d) Period 6.

The important information in these graphs is the slopes of the un-cleaned modules versus the EDS equipped modules (the difference of slopes is a good indicator of the efficiency of EDS).
Table 4.3 reports the soiling loss for reference modules and for modules equipped with the electrodynamic cleaning system from CleanFizz over each period and as average over the total 458 days of measurement. The relative performance loss due to soiling can vary from -0.06 %/day to -0.41 %/day for reference modules and from -0.003 %/day to -0.22 %/day for PV modules equipped with electrodynamic cleaning system (EDS). The relative soiling rate performance reduction varies from 17.5% to 95.7% with an average reduction of 32.1%. This result means that the electrodynamic cleaning system is well adapted for the tested soiling conditions at all time.
Comparing the indoor and the field tests, a difference in efficiency can be observed. This could have various origins like (1) the improvement brought to new indoor electrodes compared to the field test generation, (2) the shape and size of the dust can be different from the tested sand, and finally (3) the cementation of the dust with presence of moisture due to condensation [24], as this was not evaluated during the indoor test.
As the test prototypes (40x50 cm^2) are smaller than the standard 72 cells panel (100x200 cm^2), effect of EDS might be underestimated as the accumulation observed in small modules is more homogeneous.

Table 4.3. Comparison of soiling losses of the reference and of the modules equipped with the CleanFizz electrodynamic cleaning system over the different periods and cost calculation of washing for both

modules. The optimal periods between washings are calculated based on electricity prices of 0.06 $/kWh and washing cost of 1300 $/MWp. For cost calculation, the price of electricity is 0.06 $/kWh, for Scania the washing cost is 1300 $/MWp and for Young the washing cost is 3000 $/MWp.

	Period	P1	P2	P3	P4	P5	P6	Average
	Number of days (days)	61	144	50	56	110	37	458
Ref	**Soiling loss ref (%/day)**	**-0.32%**	**-0.31%**	**-0.063%**	**-0.09%**	**-0.09%**	**-0.41%**	**-0.21%**
	T_{ref}: Days between washing Ref module (days)	47.7	48.4	107.2	87.5	89.4	41.9	68.8
With EDS	**Soiling loss with EDS (%/day)**	**-0.24%**	**-0.25%**	**-0.003%**	**-0.06%**	**-0.07%**	**-0.20%**	**-0.15%**
	T_{EDS}: Days between washing EDS module (days)	55.0	53.2	514.9	111.8	99.6	60.7	122.8
	Difference of soiling loss (%/day)	-0.08%	-0.06%	-0.06%	-0.03%	-0.02%	-0.21%	-0.06%
	Relative difference of soiling loss (%/day)	**24.8%**	**17.5%**	**95.7%**	**38.7%**	**19.4%**	**52.3%**	**32.9%**
Cost Calculations								
Scania [24]	Gain in washing cost with EDS per year $/MW/y	1324.1	899.4	3505.0	1175.3	543.8	3505.7	1399
	Gain in washing cost with EDS over 20y $/module (380 Wp)	**10.1**	**6.8**	**26.6**	**8.9**	**4.1**	**26.6**	**10.4**
Young [25-26]	Gain in washing cost with EDS per year $/MW/y	2011.5	1366.2	5324.5	1785.4	826.1	5325.6	2126
	Gain in washing cost with EDS over 20y $/module (380 Wp)	**15.3**	**10.4**	**40.5**	**13.6**	**6.3**	**40.5**	**16.2**

3.5.3 Cleaning cost calculation and electrodynamic cleaning system (EDS) gain

Soiling causes important revenue losses of the utility scale PV power plan. A simple approach gives the optimal time between each wash (T in days) based on cost calculation, which includes r, the rate of revenue loss in $/day^2 and W, the cost of a single wash of the PV modules for the full installation in $ [25, 26]:

$$T = \sqrt{\frac{2W}{r}}$$

This optimal time between washing sessions is based on following hypothesis:

- The rate of revenue loss *r* due to soiling is constant.
- Washing restores power generation to 100%.
- Seasonal as well as weather influences are ignored.

r is calculated as the product of the power of installation in Wp, the price of electricity in $/Wh and the number of hours at 1 sun per day (approximated by the ratio of the integral of I_{sc} (45 ± 5 Ah) and $I_{sc(max)}$ (7.5 ± 0.5), which gives 6 ± 1.07 h/day).

To have a linear rate, short periods (without manual cleaning) are considered to calculate the optimal time between cleanings: first for reference modules and then for EDS equipped modules (Table 4.3).

The modules including EDS show systematically a longer time between washes, meaning a cost saving all over the year. That can be extrapolated over the lifetime warranty of a solar panel (20 years) to obtain the cost saving on washing (CSW) when using the electrodynamic cleaning system (EDS).
Fig. 4.30 shows a cost estimation study of the CSW using EDS based on average soiling rate over the total period studied: -0.21 %/day for reference modules and -0.15 %/day for modules equipped with EDS the relative reduction of loss is -32.1%. As a reference, a washing cost of 1300 $/MW and an electricity price of 0.06 $/kWh are used, which gives a CSW over module lifetime of 20 years of 10.6 $/module (based on a 72 cells module of 380 Wp and a surface of 2 square meters, 19% in efficiency). Considering an electricity price of 0.22 $/kWh, the added value of EDS can reach 20 $/module (at 1300 $/MW of conventional washing cost). Similarly with a washing cost of 4500 $/MW, the calculated added value of EDS is also 20 $ with an electricity price of 0.06 $/kWh).

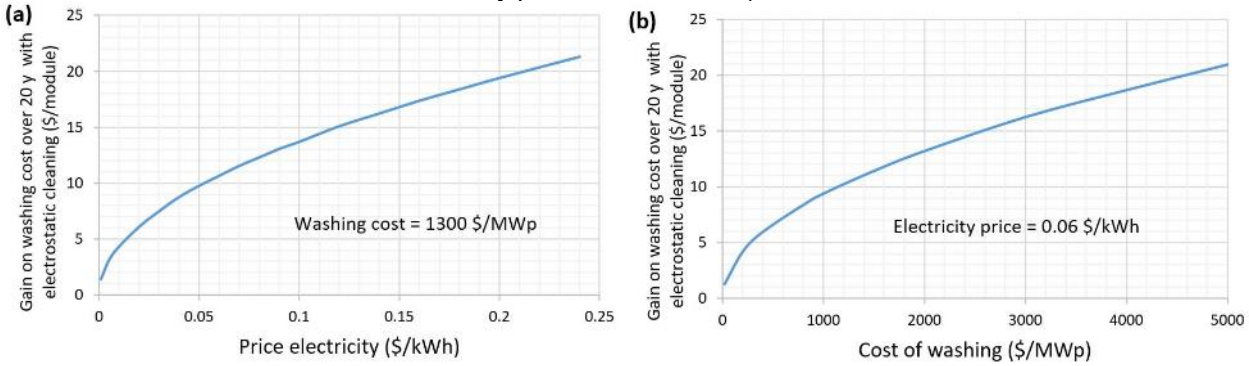

Fig. 4.30. Cost saving estimation study using electrodynamic cleaning system (EDS) based on data collected in Table 3 versus (a) electricity price and (b) washing cost for 72 cells module of 380 Wp.

At KAUST, with the PV module conditions considered, the EDS will have a cost limit between 10 and 20 $/module of 72 cells, which gives when related to power a gain of 2.6 to 5.2 ¢/Wp, which is already about 10% to 20% of the module cost. The calculated cost of the EDS should include electrode fabrication, interconnection and high voltage pulsed source.
It is important to note that EDS can also save an important quantity of fresh and clean water used for washing of solar plans installed in arid regions. For example, the cleaning of 1 MWp (mega-watt-peak) PV power plan in Atacama Desert consumes the same amount of water as a typical village, with 1.2 washing a month and 2 liters per square meter for each wash, then at total of about 151 m^3/year/MWp of water is needed [27]. Using the electrodynamic cleaning system, the water consumption can be reduced from 10 to 80% depending on the soiling rate (see Table 4.3). The reduction of the annual consumption from 151 to only 30 m^3/MWp would be of great interest for regions with scares water supply. Further tests will be implemented to see the efficiency of EDS in Chile desert.

4 Conclusions and outlook

This project shows the feasibility of large-scale fabrication of anti-soiling electro-dynamic cleaning system (EDS) integrated on standard PV modules. Wire-electrode (WE) connected with printed circuit board is the choice for the up-scaling of EDS as this can be used both for cleaning and heating. Heating a PV module avoid dew point at the module surface and water condensation at module surface. When the dust particles are wet due to water condensation, this create cementation of the dust which make it very difficult to remove or clean. Heating the module by joule effect through the WE is more efficient than using the cells with forward current as the WE is closer to the top surface compared to the cells.

Cleaning efficiency is influenced by many factors that can be separated in 3 groups: 1. Outdoor conditions, 2. High voltage electronics parameters and 3. Electrode design. For the first group (outdoor condition), it is clear that the dust type has a large influence in particular the particle size of the dust, the particles size between 1 and 200 microns are efficiently cleaned for larger of smaller particles variation of the EDS system need to be further studied. The dust loading in grams per square meter is also an important factor, at large load the particles accumulation stop EDS cleaning. For that a good control of the cleaning is needed to avoid sand accumulation.

The field test show that the gain in cleaning cost can be between 9 and 22 CHF/module over its full life, this gives a good starting point for cost evaluation of the EDS electrode and electronics value.

4.1 Next steps after end of project

Next steps are to sell the Dust Buster to different R&D institute or R&D centres for large companies that are working or interested to work on soiling for PV and CSP applications. The Dust Buster is also a good advisory product for anti-soiling electro-dynamic cleaning system. The best way to make people interested in a technology is to make people testing the technology.

The other next steps are to find investors for setting a line of module including anti-soiling EDS technology. A good combination would be to bring together the low thermal coefficient of silicon heterojunction solar cells and the anti-soiling technology.

5 Publications [within the project]

CSEM_2019_1 *ElectroDynamic System (EDS) as anti-soiling technology for PV modules & systems*, A. Faes, D. Petri, J. Champliaud, J. E. Palou, N. Badel, J. Geissbühler, B. Roustom, G.-O. Getaz, G. McKarris, A. Hessler-Wyser, N. Wyrsch, M. Despeisse, C. Ballif, Visual presentation, PV-Tagungs, Bern, 24.03.2019.

CSEM_2019_2 *Field test and electrode optimization of electrodynamic cleaning systems for solar panels,* A. Faes, D. Petri, J. Champliaud, J. E. Palou, N. Badel, J. Geissbühler, B. Roustom, J. Levrat, G.-O. Getaz, G. McKarris, A. Hessler-Wyser, N. Wyrsch, M. Despeisse, C. Ballif, Progress in Photovoltaics, Volume27, Issue11, Special Issue: EU PVSEC Papers, Pages 1020-1033, DOI: 10.1002/pip.3176, November 2019.

CSEM_2020_1 *Anti-soling for PV module & System: ElectroDynamic System (EDS)*, A. Faes, D. Petri, J. Champliaud, J. E. Palou, N. Badel, J. Geissbühler, B. Roustom, G.-O. Getaz, G. McKarris, A. Hessler-Wyser, N. Wyrsch, M. Despeisse, C. Ballif, Visual presentation, PV-Tagungs, Lausanne, 24.03.2020.

6 References

[1] Aïssa B, Isaifan RJ, Madhavan VE, Abdallah AA. Structural and physical properties of the dust particles in Qatar and their influence on the PV panel performance. Sci Rep 2016;6:31467.

[2] Mesbahi M. Soiling: origin, measurements, analysis & solutions. Solar Asset Management, Solarplaza 2018.

[3] Cohen Segev A. India's need for water free solar panel cleaning. Energetica India, Aug 2015;4.

[4] Mazumder MK, Horenstein MN, Joglekar NR, Sayyah A, Stark JW, Bernard AAR, Garner SM, Yellowhair JE, Lin HY, Eriksen RS, Griffin AC, Gao Y, La Centra R, Lloyd AH. Mitigation of dust impact on solar collectors by water-free cleaning with transparent electrodynamic films: progress and challenges. IEEE J Photovolt 2017;7:7:1342-1352

[5] Kawamoto K, Shibata T. Electrostatic cleaning system for removal of sand from solar panels. J. Electrostat 2015;73:65-70.

[6] Guo B, Javed W. Efficiency of electrodynamic dust shield at dust loading levels relevant to solar energy applications. IEEE J Photovol. 2018;8:1:196-202.

[7] Masuda S, Fujibayashi K, Ishida K, Inaba H. Confinement and transportation of charged aerosol clouds via electric curtain, Trans. Inst. Electr. Eng. Jpn 1972;92:9-18.

[8] Calle CI, Buhler CR, McFall JL, Snyder SJ. Particle removal by electrostatic and dielectric forces for dust control during lunar exploration missions, J. Electrostat. 2009;67:89-92.

[9] Robison JR, Sharma R, Zhang J, Mazumder MK. Computer simulation of electrodynamic screens for mars dust mitigation, in: Proc. ESA Annual Meeting on Electrostatics, 2008. Paper A3.

[10] Onozuka M, Ueda Y, Oda Y, Takahashi K, Seki Y, Aoki I, Ueda S, Kurihara K. Development of dust removal system using static electricity for fusion experimental reactors, J Nucl Sci Technol 1997;34:1031-1038.

[11] Schmidlin FW, A new nonlevitated mode of traveling wave toner transport, IEEE Trans. Ind. Appl. 1991;27:480-487.

[12] Taniguchi K, Morikuni S, Watanabe S, Nakano Y, Sakai T, Yamamoto H, Yagi T, Yamamoto Y. Improved driving characteristics for the toner transportation system, in: Proc., NIP16: Int. Conf. on Digital Printing Technologies, Society for Imaging Science and Technology, Springfield, VA, 2000;740-742.

[13] Aoyama M, Oda T, Ogihara M, Ikegami Y, Masuda S, Electrodynamical control of bubbles in dielectric liquid using a non-uniform traveling field, J. Electrostat. 1993;30:247-258.

[14] Masuda S, Washizu M, Kawabata I, Movement of blood cells in liquid by nonuniform traveling field, IEEE Trans. Ind. Appl. 1988;24:217-222.

[15] Mazumder M, Herenstein M, Stark J, Erickson D, Sayyah A, Jung S, Hao F. Development of self-cleaning solar collectors for minimizing energy yield loss caused by dust deposition. In proc. ASME 7th Int Conf Ene Sust, 2013;18365

[16] Kawamoto H, Uchiyama M, Cooper BL, McKay DS, Mitigation of lunar dust on solar panels and optical elements utilizing electrostatic traveling-wave. J. Electrostat. 2011;69:370-379.

[17] Chesnutt JKW, Ashkanani H, Guo B, Wu CY. Simulation of microscale particle interactions for optimization of an electrodynamic dust shield to clean desert dust from solar panels. Sol. Energy Mater Sol. Cells. 2017;155:1197–1207.

[18] Mazumder MK, Horenstein MN, Stark JW, Girouard P, Sumner R, Henderson RB, Sadder O, Hidetaka I, Biris AS, Sharma R. Characterization of electrodynamic screen performance for dust removal from solar panels and solar hydrogen generators. IEEE Trans. Ind. Appl. 2013;49:4:1793–1800.

[19] Geissbühler J, De Wolf S, Faes A, Badel N, Jeangros Q, A. Tomasi A, L. Barraud L, A. Descoeudres A, M. Despeisse M, Ballif C. Silicon heterojunction solar cells with copper-plated grid electrodes: Status and comparison with silver thick-film techniques. IEEE J. Photovolt, 2014;4:4:1055.

[21] Kawamoto H, Guo B. Improvement of an electrostatic cleaning system for removal of dust from solar panels. J. Electrostatics, 2018;91:28-33.

[22] Javed W, Wubulikasimu Y, Figgis B, Guo B. Characterization of dust accumulated on photovoltaic panels in Doha, Qatar, Sol. Energy, 2017;142:123-135.

[23] Ilse KK, Figgis B, Naumann V, Hagendorf C. Dew as a detrimental influencing factor for soiling of PV modules In IEEE 7-WCPEC, Soiling 1, Waikoloa, June 2018

[24] Enbar N, Wenig D, Klise G. Budgeting for solar PV plant operation & maintenance: Practices and pricing, Electric Power Research Institute, Sandia Laboratories, December 2015, www.epri.com.

[25] Young D, Solarrus Corp., “To Wash or Not to Wash? Framework for Making an Informed Decision”, Solar O&M: NA Workshop, San Francisco, March 25-26, 2014

[26] Klause MB, 14 April 2014, https://www.greentechmedia.com/articles/read/do-you-wash-your-solar-modules-often-enough.

[27] Cabrera E, Schneider A, Wefringhaus E, Rabanal J, Ferrada P, Thaller D, Araya F, Marzo A, Trigo M, Olivares D, Haas J, Fuentealba E, Kopecek R, Advancements in the Development of ‘‘AtaMo’’: A Solar Module Adapted for the Climate Conditions of the Atacama Desert in Chile - The Impact of Soiling and Abrasion. in proc. 32nd EU PVSEC, p.1573 10.4229/EUPVSEC20162016-5BO.11.5

7 Appendix

7.1 Appendix 1: Copy of the paper publish during the project

Field test and electrode optimization of electrodynamic cleaning systems for solar panels, A. Faes, D. Petri, J. Champliaud, J. E. Palou, N. Badel, J. Geissbühler, B. Roustom, J. Levrat, G.-O. Getaz, G. McKarris, A. Hessler-Wyser, N. Wyrsch, M. Despeisse, C. Ballif, Progress in Photovoltaics, Volume27, Issue11, Special Issue: EU PVSEC Papers, Pages 1020-1033, DOI: 10.1002/pip.3176, November 2019.